Epithelial-specific isoforms of protein 4.1R promote adherens junction assembly in maturing epithelia

Received for publication, June 4, 2019, and in revised form, November 20, 2019 Published, Papers in Press, November 27, 2019, DOI 10.1074/jbc.RA119.009650

Shu-Ching Huang[‡§¶1], Jia Y. Liang[‡], Long V. Vu[‡], Faye H. Yu[‡], Alexander C. Ou[‡], Jennie Park Ou[‡], Henry S. Zhang[‡], Kimberly M. Burnett[‡], and Edward J. Benz, Jr.[‡§¶‖]**

*From the [‡]Department of Medical Oncology, Dana-Farber Cancer Institute, the [§]Department of Medicine, Brigham and Women's Hospital, the Departments of [¶]Medicine and [‖]Pediatrics and Genetics, Harvard Medical School, and the **Dana-Farber/Harvard Cancer Center, Boston, Massachusetts 02115*

Edited by Enrique M. De La Cruz

Epithelial adherens junctions (AJs) and tight junctions (TJs) undergo disassembly and reassembly during morphogenesis and pathological states. The membrane–cytoskeleton interface plays a crucial role in junctional reorganization. Protein 4.1R (4.1R), expressed as a diverse array of spliceoforms, has been implicated in linking the AJ and TJ complex to the cytoskeleton. However, which specific 4.1 isoform(s) participate and the mechanisms involved in junctional stability or remodeling remain unclear. We now describe a role for epithelial-specific isoforms containing exon 17b and excluding exon 16 4.1R ($4.1R^{+17b}$) in AJs. $4.1R^{+17b}$ is exclusively co-localized with the AJs. $4.1R^{+17b}$ binds to the armadillo repeats 1–2 of β-catenin via its membrane-binding domain. This complex is linked to the actin cytoskeleton via a bispecific interaction with an exon 17b–encoded peptide. Exon 17b peptides also promote fodrin–actin complex formation. Expression of $4.1R^{+17b}$ forms does not disrupt the junctional cytoskeleton and AJs during the steady-state or calcium-dependent AJ reassembly. Overexpression of $4.1R^{-17b}$ forms, which displace the endogenous $4.1R^{+17b}$ forms at the AJs, as well as depletion of the $4.1R^{+17b}$ forms both decrease junctional actin and attenuate the recruitment of spectrin to the AJs and also reduce E-cadherin during the initial junctional formation of the AJ reassembly process. Expressing $4.1R^{+17b}$ forms in depleted cells rescues junctional localization of actin, spectrin, and E-cadherin assembly at the AJs. Together, our results identify a critical role for $4.1R^{+17b}$ forms in AJ assembly and offer additional insights into the spectrin–actin–4.1R-based membrane skeleton as an emerging regulator of epithelial integrity and remodeling.

Epithelial cells attach to one another through their lateral membranes and organize as single cell layered epithelial sheets that form boundaries between different environments within a tissue so that the exchange of nutrients and metabolites is tightly controlled (1). The assembly of adhesive contacts at discrete contact regions between neighboring cells is critically important for the integrity and barrier properties of epithelial layers. Cell–cell adhesion in epithelial cells is facilitated by several junctional complexes, such as tight junctions (TJs),[2] adherens junctions (AJs), and desmosomes that span the lateral plasma membrane and interact with the corresponding junctions from the opposite cell (2). The establishment of AJs is generally a prerequisite for the development and maintenance of TJs and desmosomes (3). These cell–cell junctions play indispensable roles in regulation and control of epithelial cell polarization, tissue morphogenesis, differentiation, proliferation, and motility (4).

AJs are a central feature of epithelial sheets and consist of multiple protein complexes. The major component of the AJs is the cadherin–catenin adhesion complex that serves as a bridge connecting the actin cytoskeleton of adjacent cells. The single-pass transmembrane E-cadherin molecule forms homo-*cis*-dimers; their *trans*-interactions through the extracellular region trigger cell–cell adhesion. Upon establishment of intercellular contacts, E-cadherin clusters and stabilizes at the plasma membrane via interaction between the cytoplasmic tail of E-cadherin and cytosolic scaffold proteins α, β, and p120-catenin, which in turn link to the actin cytoskeleton (5, 6). Binding of additional regulatory proteins and signaling molecules results in a mature AJ (7). The variety of protein interactions utilizing the AJ platform provides for the delicate regulation of AJ complexes. Cadherin-mediated cell–cell contacts increase the junctional stability that is critical for epithelial sheet integrity and function. The AJ is also highly dynamic, enabling reorganization and cell movement in epithelial and endothelial tissues. Embryonic development and epithelial–to–mesenchymal transition require the regulation and restructuring of cell adhesions through cadherins (8). A continuous remodeling of junctional complexes is closely associated with changes in cell size,

This work was supported by National Institutes of Health Grants HL44985 and HL24385 (to E. J. B.) and HL60519 and a Claudia Barr Award (to S. C. H.). The authors declare that they have no conflicts of interest with the contents of this article. The content is solely the responsibility of the authors and does not necessarily represent the official views of the National Institutes of Health.

[1] To whom correspondence should be addressed: Dept. of Medical Oncology, Dana-Farber Cancer Institute, 450 Brookline Ave., Boston, MA 02215. Tel: 617-632-6965; Fax: 617-632-4850; E-mail: shu-ching_huang@dfci.harvard.edu.

[2] The abbreviations used are: TJ, tight junction; 4.1R, protein 4.1R; AJ, adherens junction; DMEM, Dulbecco's modified Eagle's medium; GST, glutathione *S*-transferase; PVDF, polyvinylidene difluoride; FERM, 4.1/Ezrin/Radixin/Moesin; NF2, neurofibromatosis 2; bp, base pair; Ab, antibody; HP, headpiece; MBD, membrane-binding domain; CTD, C-terminal domain; NTD, N-terminal domain; ARM, armadillo domain; $4.1R^{+17b}$, exon 17b-containing 4.1R; RFP, red fluorescent protein; MDCK, Madin-Darby canine kidney; Ab, antibody; SAB, spectrin–actin binding domain; EGFP, enhanced GFP; GAPDH, glyceraldehyde-3-phosphate dehydrogenase; aa, amino acid; HUVEC, human umbilical vein endothelial cell.

cell shape, and cell movement that occur during normal epithelial morphogenesis and diseased tissue repair (9–12).

The dynamics of AJs require the coordinated interplay between the reorganization of the peri-junctional F-actin cytoskeleton and the remodeling of the plasma membrane (9, 10, 13). The linkage of the AJ complex to actin filaments forms AJ–cytoskeletal intersections critical for transducing signals that in turn enable cells to sense and respond to physical changes in their environment and drive the remodeling of epithelial junctions (9–12, 14).

Several lines of evidence support the role of actin filaments in regulation of AJs. Disruption of actin filaments causes rapid AJ disassembly (15, 16) and impairs re-establishment of intercellular contacts (11, 17, 18). Studies of the reorganization of the cadherin–catenin complex in AJs have identified actin-polymerizing, bundling, and motor proteins associated with AJs. For example, formin-1 is an actin nucleator that binds α-catenin and localizes to AJs (19), and cortactin is recruited to cell–cell adhesive contacts and binds to p120-catenin upon homophilic cadherin interaction (20). Disruption of the α-catenin–formin-1 interaction blocks assembly of radial actin cables and perturbs intercellular junction adhesion (19). Inhibition of cortactin activity reduces E-cadherin–mediated contact formation and actin reorganization (21).

Molecular details of the interactions between the epithelial AJ and the peri-junctional actin cytoskeleton have recently emerged. Various molecular components of the membrane skeleton have been implicated in linking the actin filaments to the cytosolic face of the plasma membrane. Among them, the significance of the spectrin skeleton has been well-documented. Spectrin links a number of filament systems to the cell membranes and contributes to membrane organization and stability (22, 23). In erythrocytes, spectrin–actin membrane skeletal proteins link to the plasma membrane and play a critical role in maintaining cell morphology and membrane mechanical properties (23). In epithelial cells, spectrin assembled in the regions of cadherin-mediated cell–cell contacts are essential for formation of a stable contact (24). Studies on AJs revealed the importance of the spectrin-based membrane skeleton in epithelial morphogenesis; depletion of spectrin results in AJ disassembly in follicle epithelia in *Drosophila* (25). Junctional recruitment and stabilization of βII-spectrin at the cell–cell contact are critical for the formation of AJs in human epithelia (26).

Spectrins are composed of two α- and β-spectrin heterodimers and assemble as tetramers that weakly bind to actin at each end. Several accessory proteins, such as ankyrin-G (27), adducin (26, 28), and FERM (4.1, ezrin, radixin, and moesin) family proteins (29–31), not only enhance the association of spectrin with actin filaments but also link spectrin to the plasma membrane through their dual affinity for the spectrin–actin cytoskeleton and the cytoplasmic domains of transmembrane proteins (22, 23). Ankyrin-G binds to the cytoplasmic domain of E-cadherin, recruits βII-spectrin to E-cadherin/β-catenin complexes, and links to the actin cytoskeleton (27). The coordinated effects of ankyrin-G and βII-spectrin are required for membrane biogenesis and proper AJ assembly in both cultured cells and mouse embryos (27). Adducin possesses actin filament bundling and capping activities (32, 33). It mediates the recruitment of spectrin to actin filaments and co-localizes with E-cadherin/β-catenin at AJs. The spectrin–adducin-based membrane skeleton serves as an important regulator of AJ integrity and remodeling (28). Its disruption impairs formation of the highly-ordered spectrin lattice at the plasma membrane of contacting cells and results in attenuated junctional assembly.

FERM proteins support the linkage between proteins attached to or embedded in the plasma membrane and the underlying actin cytoskeleton and stabilize E-cadherin–containing cell–cell contacts (30). The neurofibromatosis 2 (NF2) tumor suppressor protein, merlin, interacts with βII-spectrin and is directly involved in actin–cytoskeleton organization (31). NF2 deficiency promotes tumorigenesis and metastasis by destabilizing AJs (30). Protein 4.1R (4.1R) is a molecular scaffold in the membrane skeleton that stabilizes the spectrin–actin network at the plasma membrane (23). Erythroid differentiation stage-specific inclusion of exon 16 generates 4.1R isoforms vital for the stabilization of the spectrin–actin complex and for the maintenance of the red blood cell cytoskeleton (34, 35). Exon 16–encoded peptides are also required to stimulate fodrin/F-actin association in nonerythroid cells (36). It has been recognized that 4.1R forms are enriched at cell–cell contacts in cultured epithelial cells (37) and mouse gastric epithelial cells (38). 4.1R is expressed as a diverse array of isoforms, within which the expression of exon 17b–containing forms is epithelial cell-specific (39) and localized at the AJs (38). 4.1R has been shown to link the AJ complex to the cytoskeleton. Histological examination revealed that cell–cell contacts are impaired, and gastric glands are disorganized in 4.1R null stomach epithelia (38). The spectrin–actin–4.1R-based membrane skeleton and adherens junctional affiliation are well-recognized, but the specific role of 4.1R remains poorly understood.

Studies on the structure–function relationships involving a plethora of 4.1R isoforms have resulted in elucidation of the diverse functions of 4.1R in cellular processes, such as in mRNA splicing (40), nuclear assembly (41), cell division (42, 43), and interaction with components of the contractile apparatus in skeletal myofibers (44). Similarly, AJs consist of multiple protein complexes; within each component, multiple isoforms have been identified. For example, cadherin isoform switching occurs during the epithelial–to–mesenchymal transition, which allows cell types to separate from one another (45). Different roles of p120–catenin isoforms are linked to cell viability, proliferation, and invasiveness in carcinogen-induced rat skin tumors (46). Furthermore, the Ca^{2+}-independent adhesion molecule nectin and an actin filament–binding afadin localize at cadherin-based AJs. Afadin has two splice variants: l-afadin has an actin filament-binding domain, whereas s-afadin lacks this domain (47). The challenge is to identify the precise roles of each specific isoform of each component expressed in AJs in order to understand the AJ physiology. This report focuses on the 4.1R component.

In this study, we examined the role of 4.1R in remodeling of AJs in cultured MDCK epithelial cells. We now describe the function of epithelial-specific exon 17b–containing 4.1R ($4.1R^{+17b}$) forms in AJs. $4.1R^{+17b}$ forms are exclusively co-lo-

calized and associated with AJ proteins, linking the armadillo repeats 1–2 of β-catenin, via the 4.1R membrane-binding domain, to the actin cytoskeleton, via an exon 17b-encoded peptide. We show that $4.1R^{+17b}$ positively impacts calcium-dependent AJ assembly, most likely by governing assembly of peri-junctional F-actin bundles and recruiting βII-spectrin to the areas of cell–cell contact. Our results offer new insights into the biological function of $4.1R^{+17b}$ forms in stabilization of E-cadherin–dependent adhesion and suggest a molecular mechanism by which 4.1R modulates AJ assembly during junctional remodeling.

Results

4.1R isoforms expressed during cell density–dependent growth arrest of epithelial cells

4.1R is known to be expressed as a diverse array of isoforms transcribed from three alternative promoters coupled with alternative splicing (48, 49). We first analyzed 4.1R localization in different confluent stages of MDCK cells using an anti-exon 13 antibody that detects all 4.1R isoforms. Actively-proliferating MDCK cells exhibited intense staining of 4.1R in the interphase nucleus, spindle poles of mitotic cells, and at the sites of cell–cell contact (Fig. 1*A*). The intensity of nuclear staining decreased and eventually disappeared, while the staining in the periphery remained intense as cells achieved confluence (Fig. 1*A*). The nuclear localization of 4.1R correlated with the rapid proliferation status of cells while the predominant cell–cell contact staining of 4.1R was associated with growth-arrested cells (Fig. 1*B*). The peripheral localization of 4.1R could be reversed when cells were sub-cultured at a lower density. Thus, the localization of 4.1R in MDCK is cell density–dependent in MDCK cells.

We next characterized the 4.1R isoforms expressed in epithelial cells at each stage. 4.1R is composed of five chymotrypsin-digested domains: the headpiece (HP); membrane-binding domain (MBD); 16-kDa domain; spectrin–actin binding domain (SAB); and C-terminal domain (CTD) (Fig. 1*D*). Transcription from promoter 1A dictates exon 2′ exclusion, which omits an upstream translation initiation site (AUG-1) and produces the "small" (80 kDa) isoform (48, 49). Conversely, transcription from promoter 1B or 1C results in exon 2′ inclusion and utilization of the upstream translation initiation site (AUG-1), producing the "large" (135 kDa) isoform (Fig. 1*D*) (48, 49). We examined 4.1R isoforms expressed in MDCK by RT-PCR using primer sets that would amplify full-length coding sequences originating from either the upstream AUG-1 or the downstream AUG-2. Two major amplified bands separated by ~450 bp were detected in products transcribed from all three promoters 1A, 1B, and 1C (Fig. 1*C*). Both small and large class 4.1R forms lacked exons 3, 14, 15, and 17a. Two major splicing events affected exon 16 and 17b, and although both exons were omitted simultaneously in some form, the presence of exon 16 and 17b was mutually exclusive (Fig. 1*D*). Three 4.1R variants with either inclusion or exclusion of exons 16 and 17b from each large ($4.1R^{135}$, $4.1R^{135+16}$, and $4.1R^{135+17b}$) and small class ($4.1R^{80}$, $4.1R^{80+16}$, and $4.1R^{80+17b}$) were found to be the predominant forms. Minor forms of 4.1R demonstrated varying inclusions of exons 17b and 18. Of note, exon 16–encoded peptides are important for spectrin–actin interaction (34, 35). Exon 17b encodes 150 amino acids whose expression has been shown to be epithelial differentiation stage-specific (39) but with no known functions.

To assess changes in exon 16 and exon 17b expression during the confluence stages, a limiting cycle amplification protocol (50) was used to maintain the PCR within its linear range on RNA isolated from nonconfluent, sub-confluent, and confluent MDCK. Approximately 14.1% of exon 16-containing 4.1R mRNA was detected in nonconfluent cells. Exon 16 expression diminished as cells reached further confluence; it fell to 8.7% in sub-confluent cells and was almost completely extinguished when cells were confluent (Fig. 1*E*). In contrast, the expression of exon 17b gradually increased throughout the MDCK confluence process from 8.7% in nonconfluent to 59.7% in confluent cells (Fig. 1*E*). Thus, the inverse reciprocal exclusion of exon 16 and the inclusion of exon 17b are the major splicing events that occur during MDCK maturation.

A panel of 4.1R- the exon-specific antibodies was used to detect proteins isolated from different stages of confluence. An antibody specific for the universally expressed exon 13 detected four forms (Fig. 1*F*, *α-ex13*). A 135-kDa form is the only isoform detected in nonconfluent cells, albeit at a low expression level. In addition to the more abundant 135-kDa form, two major 160- and 100-kDa forms and a minor 80-kDa form were detected in sub-confluent cells. As cells reached confluence, both the 160- and 100-kDa forms increased while the 135- and 80-kDa forms decreased (Fig. 1*F*, *α-ex13*). The nature of these forms was analyzed with an anti-HP Ab specific for the peptides between the first and second translation initiation sites. It distinguishes 4.1R large forms (160 and 135 kDa) from small forms (100 and 80 kDa). As expected, 160- and 135-kDa forms detected by anti-ex13 Ab belong to the large 4.1R group as they also reacted with the anti-HP Ab (Fig. 1*F*, *α-HP*). However, further analyses with an α-ex16 Ab suggest that the 135 kDa from the nonconfluent cells is the sole form that contained the alternatively-spliced exon 16; no detectable forms from sub-confluent and confluent cells were observed (Fig. 1*F*, *α-ex16*). This is consistent with the RNA results that demonstrate decreased expression of exon 16 associated with increased cell confluency (Fig. 1*E*). Finally, the 160- and 100-kDa forms, but not the 135- and 80-kDa forms, reacted to an anti-ex17b antibody. In keeping with the RNA results, the 17b-containing forms were almost undetectable in nonconfluent cells, but their expression increased and represented the major forms as cells became confluent (Fig. 1*F*, *α-ex17b*). Exon 17b encodes an 150-amino acid polypeptide, which most likely accounts for the molecular weight differences between $4.1R^{135}$ and $4.1R^{160}$ and between $4.1R^{80}$ and $4.1R^{100}$.

When the intracellular localization of the identified 4.1R isoforms were examined, they all localized at the cell–cell contacts of confluent cells regardless of whether exon 16 or exon 17b was present (Fig. 1*G*). As reported previously (51), exon 5 is required for targeting 4.1R to the cell–cell contacts as isoforms without exon 5 were never detected there (Fig. 1*G*, 135^{-5}).

4.1R^{+17b} isoforms co-localize and associate with E-cadherin and β-catenin

Exon 17b expression is epithelial-specific; it is identified in differentiating but not proliferating human mammary epithelial cells (39) and in mouse gastric epithelia (38). Our results showed increased expression of exon 17b-containing 4.1R forms in confluent MDCK cells (Fig. 1). However, how exon 17b-containing 4.1R (4.1R^{+17b}) functions in epithelia has not yet been characterized.

We analyzed the localization of 4.1R^{+17b} using an exon 17b–specific antibody. It exclusively localized to the periphery of confluent cells. Calcium deprivation caused the disappearance

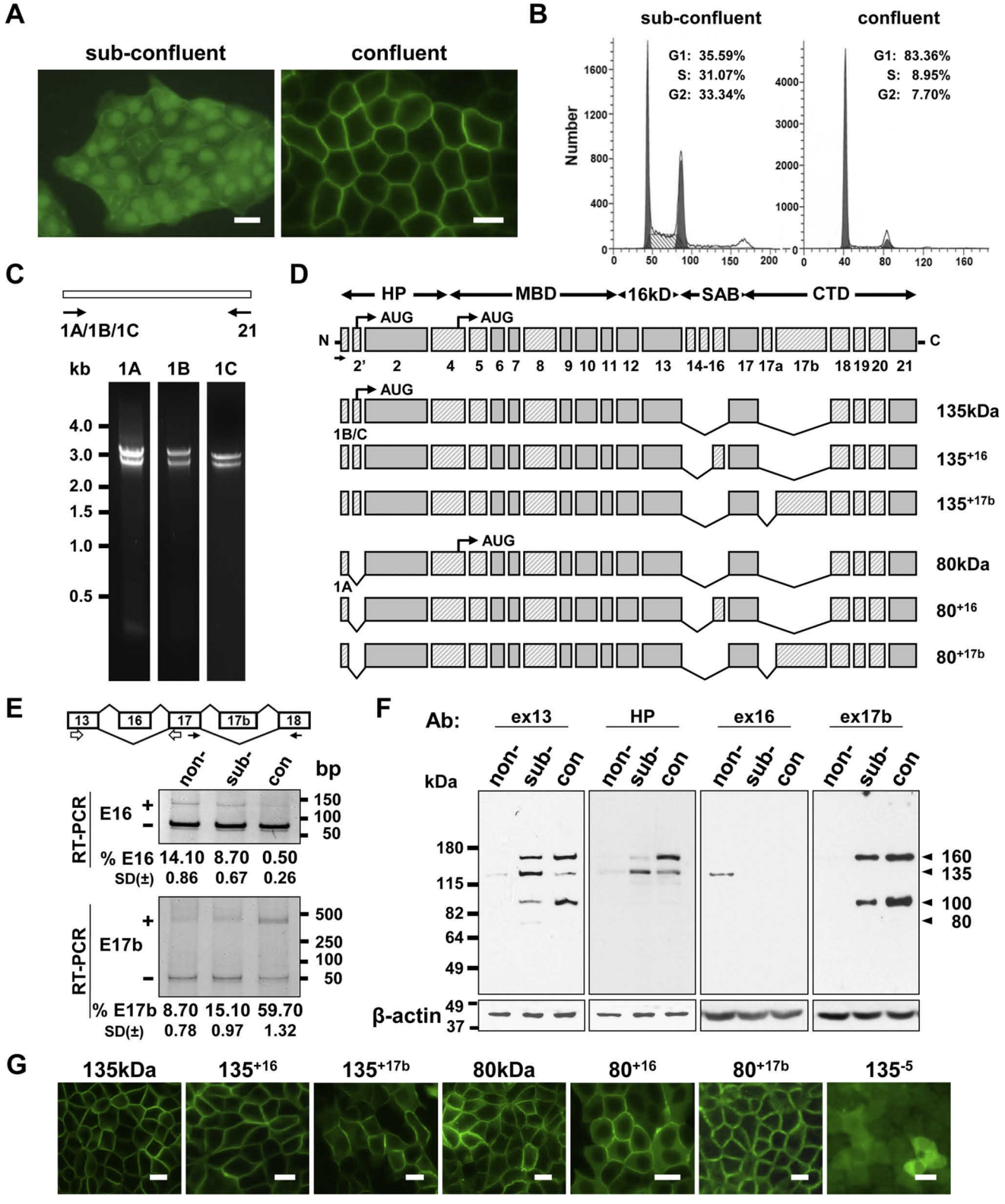

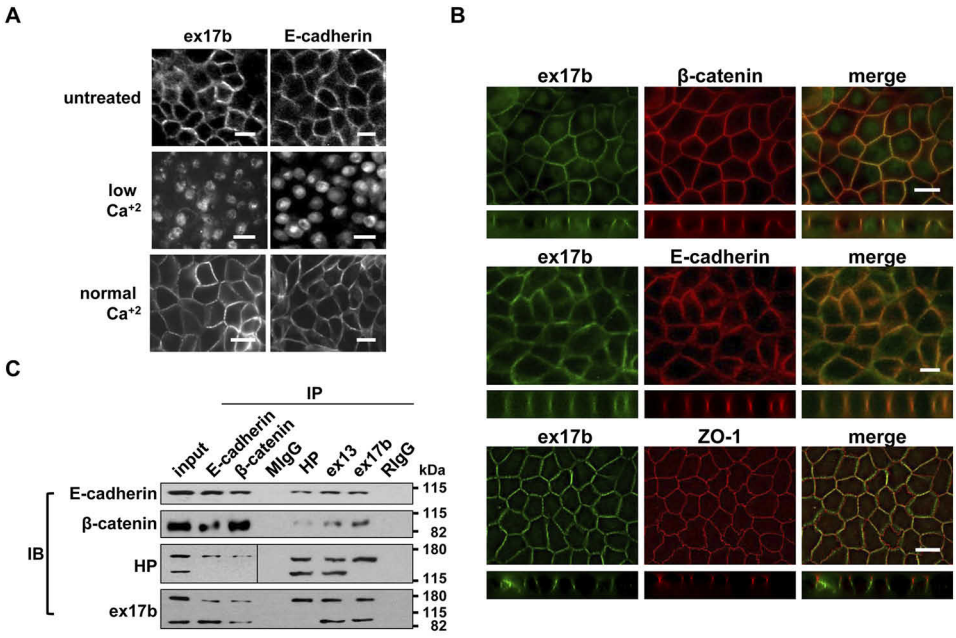

Figure 2. 4.1R^{+17b} forms localize and associate with AJ proteins in MDCK cells. *A,* subcellular localization of 4.1R^{+17b} and E-cadherin in low and normal calcium medium. MDCK cells grown to a confluent state on a coverslip in normal medium (*untreated*) were switched to low-calcium medium for 20 h (*low Ca^{2+}*) and returned to normal calcium medium for 8 h (*normal Ca^{2+}*). Cells were stained with anti-ex17b or anti-E-cadherin Abs and analyzed with Zeiss microscopy. *Bar,* 10 μm. *B*, intracellular localizations of 4.1R^{+17b}, β-catenin, E-cadherin, and ZO-1 were examined using its respective antibody in *XY* and *XZ* sections and revealed with Zeiss microscopy. *XZ* sections showed ex17b and E-cadherin or β-catenin, but not ZO-1, co-localized at the AJ. *Green*, ex17b; *red,* E-cadherin, β-catenin, or ZO-1. *Bar*, 10 μm. *C*, association of 4.1R^{+17b} and AJ proteins in co-immunoprecipitation assays. MDCK cell lysates were precipitated (*IP*) with an anti-E-cadherin, anti-β-catenin, a control mouse IgG (*MIg*), anti-HP, anti-ex13, anti-ex17b, or a control rabbit IgG (*RIg*) Ab. The input extracts and immunoprecipitates were examined by immunoblotting (*IB*) with its respective antibodies. Molecular mass markers (kDa) are provided at the *right margin* of each blot.

of 4.1R^{+17b} signal from cell–cell contact due to internalization. 4.1R^{+17b} regained its cell contact localization ~8 h after calcium replenishment (Fig. 2*A*). As with the AJ proteins, the cell–cell contact localization of 4.1R was calcium-dependent. As shown in Fig. 2*A*, E-cadherin disengaged from cell contacts in low-calcium medium and reappeared at cell–cell contacts after calcium replenishment.

We have shown that 4.1R is a component of the TJs and co-localizes with ZO-1 and ZO-2 (37). It has also been shown that 4.1R links the E-cadherin/β-catenin complex to the cytoskeleton in gastric epithelial cells (38). We then examined 4.1R^{+17b} localization relative to that of the AJs and TJs. 4.1R^{+17b} and β-catenin or E-cadherin co-localize at the cell–cell contacts (Fig. 2*B*). *XZ* projections of the images show the co-localization of 4.1R and β-catenin or E-cadherin at the AJ along the lateral membrane of the cells (Fig. 2*B*). However, 4.1R^{+17b} exclusively localized at the AJs and was not present at the TJs as no co-localization with ZO-1 was observed (Fig. 2*B*).

We subsequently examined whether 4.1R^{+17b} associated with AJ proteins in co-immunoprecipitation assays using MDCK lysates and anti-E-cadherin, anti-β-catenin, or anti-4.1R (anti-HP, anti-ex13, and anti-ex17b) Abs. All three 4.1R antibodies efficiently co-precipitated E-cadherin and β-catenin (Fig. 2*C*). In addition to precipitating itself, both E-cadherin and β-catenin Abs precipitated exon 17b-containing 160-kDa 4.1R when detected with an anti-HP Ab, including both exon 17b containing forms (160 and 100 kDa) as detected with an ex17b antibody (Fig. 2*C*, *ex17b*). These results suggest that 4.1R forms containing exon 17b and the AJ proteins β-catenin and E-cadherin associate in the same complex.

Membrane-binding domain of 4.1R interacts with the β-catenin armadillo domain repeats 1–2

The MBD of 4.1R is known to interact with β-catenin (38). We mapped the domain of β-catenin responsible for interacting with 4.1R–MBD. β-Catenin consists of an NTD that har-

Figure 1. Protein 4.1R isoform expression and localization during different confluent states of MDCK. *A*, immunofluorescence staining of 4.1R with an α-exon 13 Ab in sub-confluent and confluent MDCK cells. *Bar,* 10 μm. *B*, cell-cycle profiles of sub-confluent and confluent MDCK cells. *C*, RT-PCR 4.1R products amplified using an exon 21 antisense primer with an exon *1A*, *1B*, or *1C* sense primer generated two major species with a 450-bp difference from all sets of primers. Molecular markers (*kb*) are provided at the *left margin* of the gels. *D*, major 4.1R isoforms expressed in MDCK cells. Schematic diagram of 4.1R and its domains. Constitutive exons are indicated as *dark gray boxes*, and alternatively-spliced cassettes are depicted as *light gray boxes*. Exon numbers are indicated. *E*, reciprocal expression of exons 16 and 17b in maturing MDCK cells. Schematic representation of regions between exons 13 and 18 of 4.1R and the primer sets used in PCR. RNA isolated from nonconfluent (*non-*), sub-confluent (*sub-*), and confluent (*con-*) MDCK cells were analyzed for exon 16 (*E16*) and 17b (*E17b*) expression by RT-PCR. E16 or E17b inclusion was calculated as the percent of total RNA products containing exon 16 or exon 17b, respectively. Averages and S.D. were obtained from three independent experiments ($n = 3$) and presented at the *bottom of each lane*. Molecular markers (bp) are provided at the *right margin* of the gels. *F*, 4.1R protein isoforms expression during MDCK maturation. Lysates from different confluency MDCK probed with anti-ex13, anti-HP, anti-ex16, and anti-ex17b Abs. β-Actin served as a loading control. Molecular mass markers (kDa) are provided at the *left margin* of the blots. *G*, exon 5 is required for the localization of 4.1R at the cell–cell contacts in confluent MDCK cells. MDCK 4.1R isoforms with exon compositions as indicated in *D* were fused with EGFP, transfected into MDCK, and examined for their subcellular localization as revealed by Zeiss microscopy. *135^{-5}*, 4.1R 135-kDa form without exon 5. *Bar*, 10 μm.

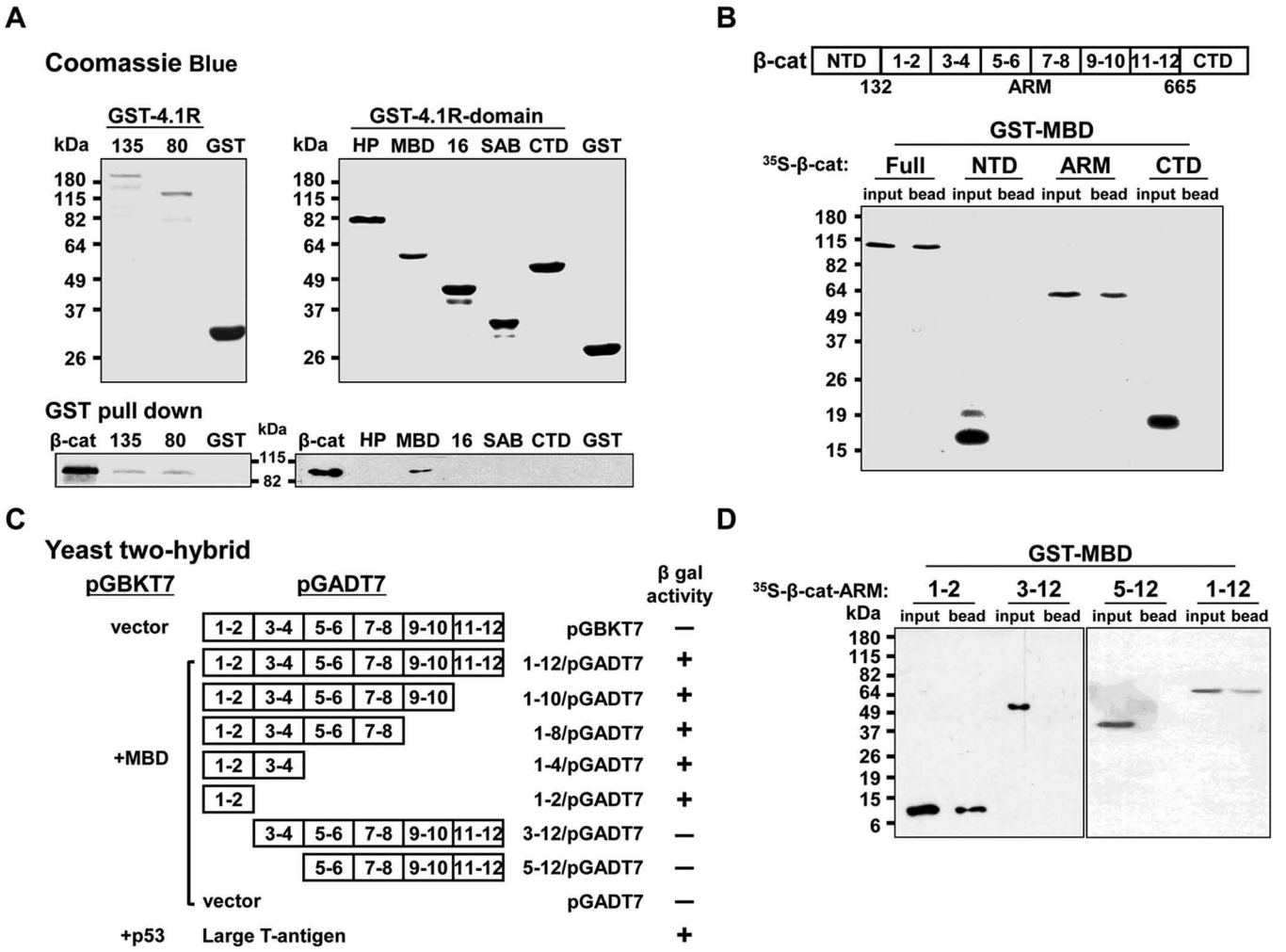

Figure 3. MBD domain of 4.1R interacts with the β-catenin armadillo domain repeats 1–2. *A*, ^{35}S-labeled *in vitro*–translated full-length β-catenin (*β-cat*) was incubated with GST–4.1R^{135} and GST–4.1R^{80} (*left*) or its individual domains (*right*) bound to GSH-Sepharose beads and analyzed for the presence of β-catenin with the GST fusions in GST-pulldown analyses. *Upper panel*, Coomassie Blue–stained GST fusions. *Lower panel*, GST-pulldown analyzed for the presence of β-catenin with GST–4.1R fusions. *B*, ^{35}S-labeled *in vitro*–translated full-length β-catenin or its individual NTD, ARM, or CTD domains were incubated with GST–MBD bound to GSH-Sepharose beads and examined for the presence of β-catenin or its domain(s) in each input and with GST–MBD fusions (*bead*). *C*, analyses of the repeats within the armadillo domain responsible for 4.1R–MBD interactions in yeast two-hybrid assays. 4.1R–MBD fused with pGBKT7 was co-transformed with the full-length armadillo domain fused with Gal4 DNA-AD in pGADT7 (*1–12/pGADT7*) or its repeat-deletion constructs (*1–10/pGADT7, 1–8/pGADT7, 1–4/pGADT7, 1–2/pGADT7, 3–12/pGADT7,* and *5–12/pGADT7*) and analyzed for β-gal activity. Transformation of pGBKT7 or pGADT7 vector without fusion protein served as a negative control. Co-transformation of p53/pGBKT7 and large T-antigen/pGADT7 served as a positive control. *D*, interaction of 4.1R–MBD and the armadillo domain repeats was confirmed in GST-pulldown analyses. ^{35}S-Labeled *in vitro*–translated full-length or its repeat-deletion β-catenin armadillo domains were incubated with GST–MBD bound to GSH-Sepharose beads and analyzed for the presence of β-catenin repeats with the GST–MBD fusions (*bead*). Molecular mass markers (*kDa*) are provided at the *left* of each blot.

bors two GSK3 phosphorylation sites (Ser-33 and Ser-37) (52), an armadillo (ARM) domain binding to axin, APC, α-catenin, BCL9, ICAT (53), and a CTD domain.

GST attached to intact 4.1R isoforms, GST attached to individual domains of 4.1R, or GST alone were bound to GSH-agarose beads, then incubated with ^{35}S-labeled *in vitro*–translated full-length β-catenin, and examined for the presence of β-catenin bound to the GST fusions. β-Catenin was detected with GST–4.1R^{135} and GST–4.1R^{80} harboring the MBD or GST–MBD but not with the HP, 16-kDa, SAB, or CTD domains (Fig. 3*A*). These results confirm the interaction between the 4.1R–MBD and β-catenin. When the full-length or the individual NTD, ARM, or CTD of β-catenin was examined for binding to 4.1R–MBD, only the full-length and ARM domain of β-catenin were detected with GST–MBD (Fig. 3*B*). The interaction of β-catenin with 4.1R–MBD is thus most likely through the armadillo domain.

The armadillo domain is composed of 12 tandem repeats that form a super-helix of helices and is proposed to mediate the interaction of β-catenin with its ligands. We then determined the repeats responsible for the 4.1R–MBD interaction in yeast two-hybrid assays. 4.1R–MBD fused with Gal4 DNA-BD vector pGBKT7 or pGBKT7 alone was co-transformed with the full-length armadillo domain fused with Gal4 DNA-AD in pGADT7 (1–12/pGADT7) or its repeat-deletion constructs (1–10/pGADT7, 1–8/pGADT7, 1–4/pGADT7, 1–2/pGADT7, 3–12/pGADT7, and 5–12/pGADT7) and analyzed for β-gal activity. The β-gal activity was detected in 1–12/pGADT7 and the partial constructs 1–10/pGADT7, 1–8/pGADT7, 1–4/pGADT7, and 1–2/pGADT7 but not 3–12/pGADT7 or 5–12/pGADT7

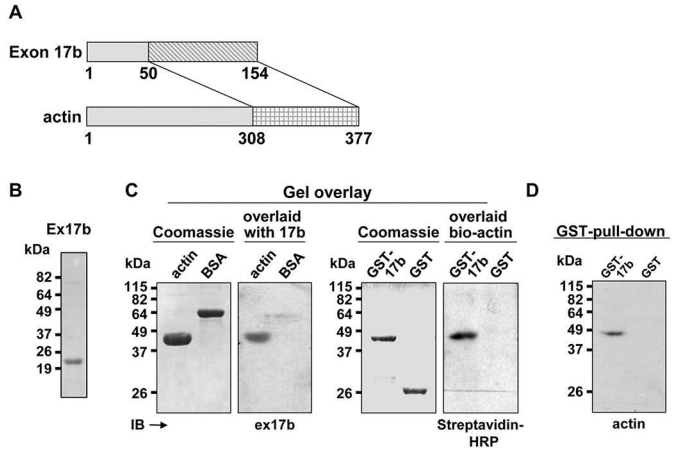

Figure 4. Exon 17b–encoded peptides interact with actin. *A*, schematic diagram of the interacting regions of exon 17b and actin. Number of amino acid residues is indicated. The 50–150 amino acids of exon 17b fused with pGBKT7 was co-transformed with a human kidney library in pGADT7 and analyzed for β-gal activity. Positive actin clones were sequenced, and the region for interacting with exon 17b peptide was identified. *B*, purified exon 17b peptides cleaved from GST–exon 17b used in gel overlay assays. *C*, blot overlay assays for the interaction between exon 17b and actin. Actin and BSA (*left*) or GST−17b and GST (*right*) are shown by Coomassie Blue staining. A duplicate gel with the same amount of proteins as in the Coomassie Blue–stained gel was separated by SDS-PAGE. Actin and BSA on the membrane were overlaid with exon 17b peptide (*left*), and GST−17b and GST on the membrane was overlaid with biotinylated actin (*right*), and followed by Western blotting with an anti-ex17b antibody (*left*) or horseradish peroxidase-streptavidin (*right*). *D*, GST-pulldown analyses for the interaction between exon 17b encoded peptide and actin. GST–exon 17b or GST immobilized on GSH-Sepharose beads were incubated with actin and analyzed for the presence of actin with the beads with an anti-actin antibody. Molecular mass markers (*kDa*) are provided at the *left margin* of each blot.

(Fig. 3*C*). These results showed that the interaction of β-catenin with 4.1R–MBD involves repeats 1–2 of the armadillo domain. The interaction between MBD and armadillo domain 1–2 repeats was further verified in GST–MBD pulldown assays (Fig. 3*D*).

Exon 17b encoded peptide interacts with actin

Exon 17b-containing 4.1R localized to the lateral membrane and co-localized and associated with β-catenin and E-cadherin (Fig. 2). No known exon 17b binding partners are known. Therefore, we analyzed exon 17b interactions in yeast two-hybrid analyses using a Match Marker pre-transformed human kidney library (Clontech). Among several interactors, the 308–377 amino acids of cytoplasmic β-actin interacted with the 50–150 amino acids of exon 17b (Fig. 4*A*). The interaction was further evaluated in gel overlay assays. Actin and BSA were fractionated by SDS-polyacrylamide gel and stained with Coomassie Blue for protein loading (Fig. 4*C*, *left*). Proteins on a replica gel were transferred to a PVDF membrane, overlaid with purified exon 17b–encoded peptides, and analyzed by Western blotting with an anti-ex17b antibody for the binding of actin to exon 17b peptide (Fig. 4*C*, *left*). Actin, but not BSA, was clearly recognized by exon 17b peptides. In a reverse gel overlay, a membrane on which fractionated GST−17b and GST was overlaid with biotinylated actin and probed with HRP-streptavidin (Fig. 4*C*, *right*). GST−17b, but not GST, was recognized by biotinylated actin. These results suggest a direct interaction between actin and exon 17b peptides. Additionally, GST-pull-down using GST−17b and actin and then subsequently probed with an anti-actin Ab also confirmed the interaction between actin with exon 17b–encoded peptide (Fig. 4*D*). The above *in vitro* experiments were performed with polymerized actin filaments; these results implicate that the exon 17b–encoded peptide is capable of binding actin in filamentous form. Taken together, these data show that exon 17b directly interacts with actin while the MBD domain interacts with armadillo domain 1–2 repeats of β-catenin, thereby connecting AJ complexes to the actin cytoskeleton.

Reduction of endogenous 4.1R^{+17b} and E-cadherin localization at the cell–cell contacts in exogenous 4.1R^{-17b}-expressing cells

4.1R^{+17b} forms not only interact with β-catenin and the actin cytoskeleton (Figs. 3 and 4) but also respond to calcium concentration in a similar manner to that of AJ proteins (Fig. 2). This led us to further analyze whether 4.1R^{+17b} forms functionally link with the epithelial AJs. MDCK cells transfected with overexpressing 4.1R isoforms with or without exon 17b identified in Fig. 1*D* (*4.1R^{135}*, *4.1R$^{135+17b}$*, *4.1R^{80}*, *4.1R^{80+17b}*) were examined for their localization compared with that of the endogenous 4.1R^{+17b} as well as in relation to that of E-cadherin or β-catenin. A mix of expressing and nonexpressing cells within the same field were analyzed for their respective differences.

In EGFP–4.1R^{135} cultures, the endogenous exon 17b was detected at the cell–cell contacts of the nonexpressing cells, but its signal was drastically reduced in the overexpressing cells where EGFP–4.1R^{135} was located (Fig. 5*A*). The *XZ* sections showed that the endogenous exon 17b–containing forms were clearly located at the lateral membrane of the nonexpressing cells but were replaced with EGFP–4.1R^{135} in the expressing cells (Fig. 5*A*, *ex17b*). When the AJ proteins were examined, E-cadherin was localized at the cell–cell contacts of the nonexpressing cells, but the signal was significantly reduced in expressing cells (Fig. 5*A*, *E-cadherin*). The *XZ* sections revealed significant reduction of E-cadherin at the AJs of EGFP–4.1R^{135}–expressing cells when compared with that of nonexpressing cells (Fig. 5*A*, *E-cadherin*). Interestingly, the lateral membrane localization of β-catenin was not altered in EGFP–4.1R^{135}–expressing cells (Fig. 5*A*, *β-catenin*) despite the reduction of E-cadherin.

Similar localization of EGFP–4.1R^{80} at the cell–cell contacts and the displacement of the endogenous 4.1R^{+17b} forms and reduction of E-cadherin from the lateral membrane were also noticed in EGFP–4.1R^{80}–expressing cells (Fig. 5*B*). The localization of AJs marker β-catenin was not affected in EGFP–4.1R^{80}–expressing cells (Fig. 5*B*). These results suggest that 4.1R^{+17b} form(s) are critical for E-cadherin localization to the lateral membrane, because its replacement with 4.1R^{-17b} forms attenuates E-cadherin localization at the AJs while having no effect on β-catenin.

To verify that the reduction in the E-cadherin signal is due to the occupation of 4.1R^{-17b} forms at the cell–cell contacts, we expressed exon 17b-containing EGFP–4.1R$^{135+17b}$ or EGFP–4.1R^{80+17b} forms and examined its effect on the localization of E-cadherin and β-catenin in similar experiments. Both EGFP–

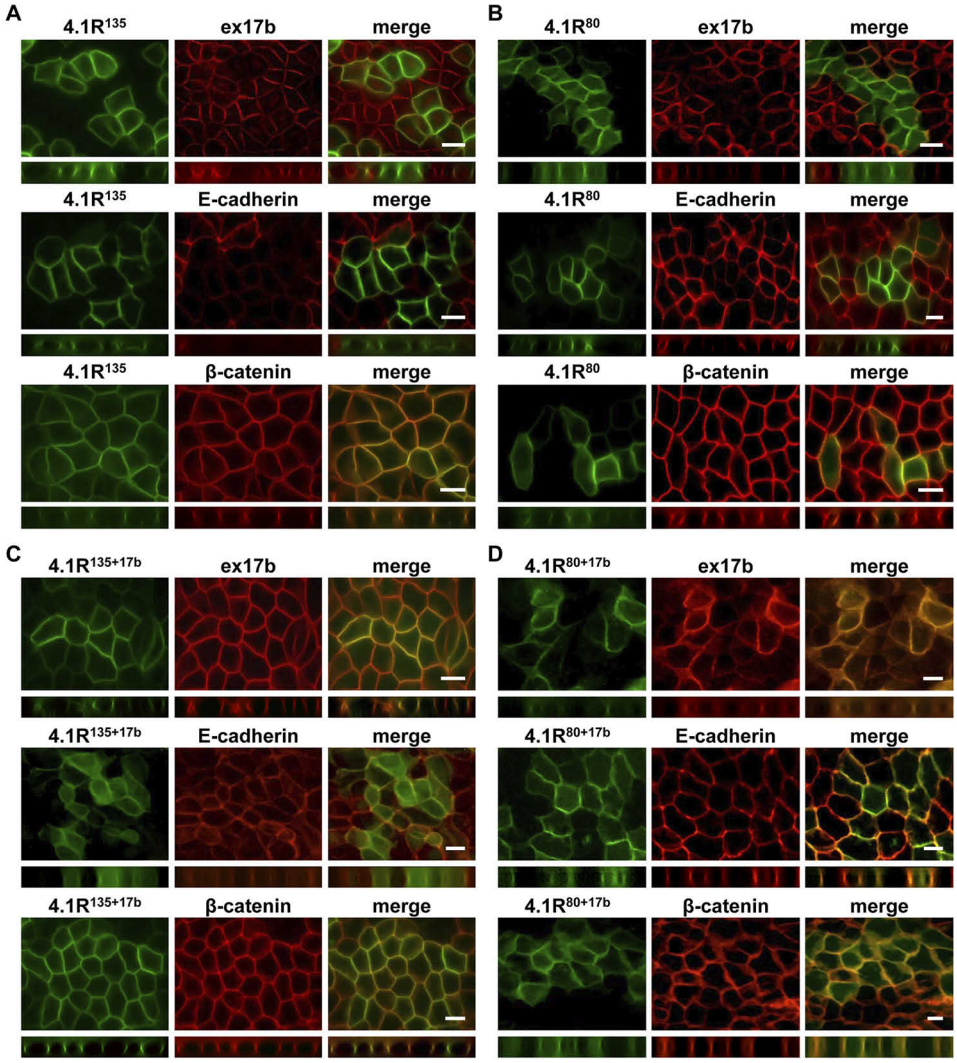

Figure 5. Reduction of endogenous 4.1R^{+17b} and E-cadherin at AJs of EGFP–4.1R^{-17b}–expressing cells but not that of EGFP–4.1R^{+17b}–expressing cells. MDCK cells were transfected with EGFP–4.1R^{135} (*A*), EGFP–4.1R^{80} (*B*), EGFP–4.1R$^{135+17b}$ (*C*), or EGFP–4.1R^{80+17b} (*D*) and immunofluorescently-stained for the presence of the endogenous 4.1R^{+17b} with an anti-ex17b and AJs with anti-E-cadherin or anti-β-catenin antibody in *XY* and *XZ* sections 36 h post-transfection and revealed with Zeiss microscopy. Regions were selected that contained a mix of transfected and untransfected cells. *A* and *B*, EGFP–4.1R^{135} (*A*) or EGFP–4.1R^{80} (*B*) displace endogenous 4.1R^{+17b} forms at cell–cell contacts (*upper*), diminish E-cadherin signals at the AJs (*middle*), but do not alter the localization of β-catenin (*lower*) at the AJs in expressing cells. *Green,* EGFP–4.1R^{135} or EGFP–4.1R^{80}; *red,* ex17b, E-cadherin, or β-catenin. *Bar,* 10 μm. *C* and *D*, expression of EGFP–4.1R$^{135+17b}$ (*C*) or EGFP–4.1R^{80+17b} (*D*) does not alter the endogenous 4.1R^{+17b}, E-cadherin, and β-catenin at the AJs of expressing cells compared with that of nonexpressing cells. *Green*, EGFP–4.1R$^{135+17b}$ or EGFP–4.1R^{80+17b}; *red,* ex17b, E-cadherin, or β-catenin. *Bar*, 10 μm.

4.1R$^{135+17b}$–expressing and -nonexpressing cells stained positive for exon 17b and localized to the lateral membrane at the cell–cell contacts as revealed in *XZ* sections (Fig. 5*C*). In contrast to EGFP–4.1R^{135}–expressing cells, EGFP–4.1R$^{135+17b}$ cells exhibited normal E-cadherin localization at the cell–cell contacts in both *XY* and *XZ* sections (Fig. 5*C*). EGFP–4.1R$^{135+17b}$ also co-localized with β-catenin at the cell–cell contacts (Fig. 5*C*). EGFP–4.1R^{80+17b}–expressing cells behaved the same way (Fig. 5*D*). These results further confirm that the occupation of 4.1R^{-17b} forms but not 4.1R^{+17b} forms at the cell–cell contacts reduce the recruitment of E-cadherin to the AJs. This is consistent with an earlier report (54) that depletion of E-cadherin does not result in noticeable AJ defects in mature junctions as the intensity and localization of β-catenin was not affected.

4.1R^{+17b} isoforms are functionally linked to reassembly of E-cadherin to the AJs

Differences in the E-cadherin signal at the cell–cell contacts observed between overexpression of 4.1R^{-17b} and 4.1R^{+17b} forms were further investigated during junctional remodeling (assembly and disassembly) in calcium-switch assays. The calcium-switch assay involved removal of extracellular calcium to trigger disassembly of preformed AJs followed by calcium re-addition to the culture medium (calcium repletion) to assemble junctional structure. Cultures with mixed expressing and non-expressing populations were analyzed in the same field for potential differences between them.

In control pEGFP-transfected cells, the EGFP signal distributed throughout the entire cell during the calcium-switch process. No differences in the distribution of E-cadherin were

found between the EGFP-expressing and -nonexpressing cells. E-cadherin localized at the cell– cell contacts in normal calcium medium (Fig. 6*A*, *NC*) and became internalized in low-calcium medium (Fig. 6*A*, *0 h*). Rapid formation of the circumferential E-cadherin at the junctions occurred 0.5 h after calcium replenishment (Fig. 6*A*, *0.5 h*). E-cadherin was well-organized to the AJ of all cells at 1 h (Fig. 6*A*, *1 h*) and continued to accumulate at the cell– cell contacts at 2 h and any time greater than 2 h after calcium replenishment (Fig. 6*A*, *2 h*). The percentage of junction assembled was scored by the ratio of the E-cadherin–

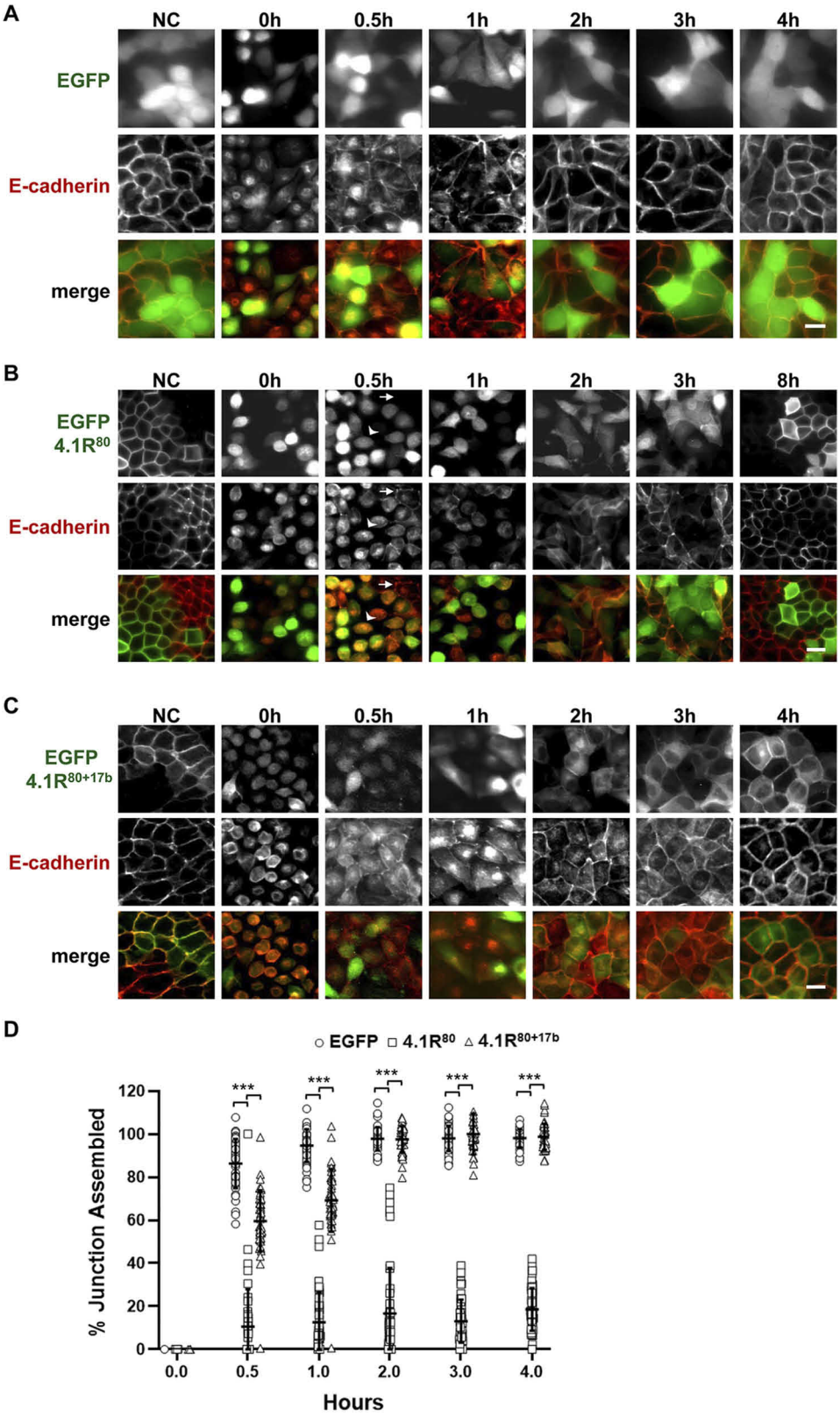

labeled length over the length of the cell periphery from 50 EGFP$^+$ cells overtime from the time course of junctional assembly. At 0.5 and 1–4 h after calcium replenishment, EGFP$^+$ cells showed ~86, 94, 97, 98, and 98% of junction assembled, respectively (Fig. 6*D*). The expression of EGFP alone did not interfere with the reassembly process of E-cadherin to the AJ.

When EGFP–4.1R^{80} cells were analyzed, significant reductions of E-cadherin at the cell–cell contacts of the expressing cells were observed when grown in normal calcium medium (Fig. 6*B*, *NC*). E-cadherin and EGFP–4.1R^{80} became internalized in both expressing and nonexpressing cells in low-calcium medium (Fig. 6*B*, *0 h*). However, substantial differences in the timing of E-cadherin appearance between the expressing and nonexpressing cells were observed during the AJ reassembly process (Fig. 6*B*). E-cadherin in nonexpressing cells, but not in expressing cells, started to organize to the cell–cell contacts 0.5 h after calcium repletion (Fig. 6*B*, *0.5 h*). Although the internalization of E-cadherin in the EGFP–4.1R^{80}–expressing cells persisted, E-cadherin organized at the cell–cell contacts of nonexpressing cells 2 h after calcium repletion (Fig. 6*B*, *2 h*). Three hours after calcium repletion, E-cadherin was completely organized at the cell–cell contacts of the nonexpressing cells but with a much less detectable signal at the cell–cell contacts of the expressing cells (Fig. 6*B*, *3 h*). The distinct E-cadherin intensity and localization pattern continued for several hours until a confluent monolayer of epithelia with cell–cell contact localization of EGFP–4.1R^{80} was formed (Fig. 6*B*, *8 h*). Reduction of E-cadherin localization at the cell–cell contacts are clearly apparent in exogenous 4.1R^{80}-expressing cells. Quantification analyses also showed that significant reduction in junction assembly was observed in EGFP–4.1R^{80}–overexpressing cells with ~10, 12, 16, 13, and 18% of junction assembled at 0.5 and 1–4 h after calcium replenishment, respectively (Fig. 6*D*). Similar reductions of E-cadherin at cell–cell contacts during the reorganization of AJ was also observed in EGFP–4.1R^{135}–expressing cells (data not shown). These results suggest that EGFP–4.1R^{-17b} localization at the cell–cell contacts prevents the recruitment of E-cadherin to cell–cell contacts at the initial reassembly and continues to interfere with mature AJ junction formation.

We then examined the EGFP–4.1R^{80+17b} culture. E-cadherin localized to the AJs of both expressing and nonexpressing cells in normal calcium medium (Fig. 6*C*, *NC*). EGFP–4.1R^{80+17b} disengaged from the membrane along with E-cadherin and became internalized in a low-calcium medium (Fig. 6*C*, *0 h*). As with control vector pEGFP-transfected cells (Fig. 6*A*), restoration of normal calcium significantly re-established the junctional localization of E-cadherin in both EGFP–4.1R^{80+17b}–expressing and -nonexpressing cells in 0.5 h and completely localized to the AJs in 2 h (Fig. 6*C*). When quantified, EGFP–4.1R^{80+17b} overexpression resulted in ~61, 70, 97, 100, and 98% junction assembly at 0.5 and 1–4 h post-calcium replenishment, respectively. Although the junction assembly was reduced at the early 0.5- and 1-h time points, junction assembly exhibited the same percentage at 2 h as that of the EGFP$^+$ cells after calcium replenishment (Fig. 6*D*). Similar reassembly of E-cadherin at the AJ was also observed in EGFP–4.1R$^{135+17b}$–expressing cells (data not shown). Taken together, these results suggest that 4.1R^{+17b} forms are important for the recruitment of E-cadherin at the initial and subsequent reassembly of the AJs.

Exon 17b-containing 4.1R forms are critical for the organization of the actin cytoskeleton and junctional recruitment of βII-spectrin

We next sought to dissect the mechanisms that might account for the observed difference in E-cadherin reassembly in 4.1R^{-17b}- and 4.1R^{+17b}-expressing cells. The membrane–cytoskeleton interface plays a crucial role in junctional reorganization. 4.1R^{135} and 4.1R^{80} forms lack both exons 16 and 17b. Given the known role of 4.1R exon 16 in regulating the spectrin-based plasma membrane skeleton (34, 36) and our findings that exon 17b–encoded peptides interact with actin, it is reasonable to postulate that expression of 4.1R forms lacking both exons 16 and 17b may have a negative effect on the organization of the membrane-associated cytoskeleton.

We first examined whether the expression of 4.1R forms affects the protein levels of the AJ and the actin cytoskeleton by evaluating the presence of E-cadherin, β-catenin, β-actin, and spectrin in EGFP–4.1R (4.1R^{80}, 4.1R^{80+17b}, 4.1R^{135}, and 4.1R$^{135+17b}$) cell lysates. No major differences in protein levels were observed in 4.1R-expressing cultures when compared with control vector-transfected cells (Fig. 7*A*).

We next analyzed whether expression of 4.1R forms lacking both exon 16 and 17b can impact epithelial junctions by affecting the organization of the spectrin lattice in the area of cell–cell contacts. Actin and βII-spectrin are closely co-localized

Figure 6. 4.1R^{+17b} forms functionally connect to the reassembly of E-cadherin at the AJs. MDCK cells transfected with pEGFP (*A*), EGFP–4.1R^{80} (*B*), or EGFP–4.1R^{80+17b} (*C*) were examined for junctional reassembly at the indicated period of time after calcium repletion in immunofluorescence-labeled analyses using an anti-E-cadherin antibody. Regions were selected that contained a mix of transfected and untransfected cells. *A*, no difference in reassembly of E-cadherin at the AJs in vector pEGFP-expressing and -nonexpressing cells. Reassembly of E-cadherin to the cell–cell contacts of both expressing and nonexpressing cells was detected 0.5 h after calcium repletion. E-cadherin continues to reassemble to AJs after 1 h and significantly accumulates at newly assembled AJs of all cells after 2 h of calcium repletion. Intense E-cadherin localizes at the AJs at 3 h and at any time greater than 3 h after calcium repletion. *B*, expression of EGFP–4.1R^{80} causes reduced E-cadherin at the cell–cell contacts of the expressing cells but not that of nonexpressing cells throughout the AJ reassembly process. Fluorescent labeling shows rapid formation of circumferential E-cadherin at the junction of the nonexpressing cells (*arrows*) but not that of expressing cells (*arrowheads*) 0.5 h after calcium repletion. The occurrence persists all the way through confluent monolayer maturation 8 h after calcium repletion. *C*, expression of EGFP–4.1R^{80+17b} does not affect the reassembly of E-cadherin at the cell–cell contacts of the expressing cells when compared with that of the nonexpressing cells. E-cadherin appears at the cell–cell contacts of all cells 0.5 h after calcium repletion. Mature monolayer cells with equal intensity of E-cadherin at AJs of all cells 3 h after calcium repletion. Composite images were generated by superimposition of the EGFP (*green*) and E-cadherin (*red*) signals; areas of overlap appear *yellow*. *Bar*, 10 μm. *D*, quantification of percent of junction assembly after calcium switch. The outline of the cell was drawn as the length of the cell periphery, and the regions of cell–cell contact labeled by E-cadherin were drawn as labeled length. Fifty EGFP$^+$ cells were measured for both cell periphery length and E-cadherin–labeled length. The percentage of junction assembled was obtained by the ratio of the E-cadherin–labeled length over the length of the cell periphery, and the data were analyzed using GraphPad Prism 8 software and expressed as mean ± S.E. of mean. *Asterisks* indicate statistical significance (***, $p < 0.001$).

with β-catenin in control MDCK cells (Fig. 7*B*). Although actin localized at the cell–cell contacts of EGFP–4.1R$^{135+17b}$–expressing cells, a slightly-reduced actin signal at the cell–cell contacts was observed in EGFP–4.1R^{135} cells (Fig. 7*C*). When βII-spectrin was examined, it accumulated at AJs in EGFP–4.1R$^{135+17b}$ cells. By contrast, βII-spectrin was retained in the perinuclear compartment, diffusely distributed over the cytoplasm, and did not completely translocate to the intercellular junctions in EGFP–4.1R^{135}–expressing cells (Fig. 7*D*). Similar differences in actin and βII-spectrin distribution were found in EGFP–4.1R^{80+17b}- and EGFP–4.1R^{80}–expressing cells (data not shown). The replacement of 4.1R^{+17b} forms by 4.1R^{-17b} at

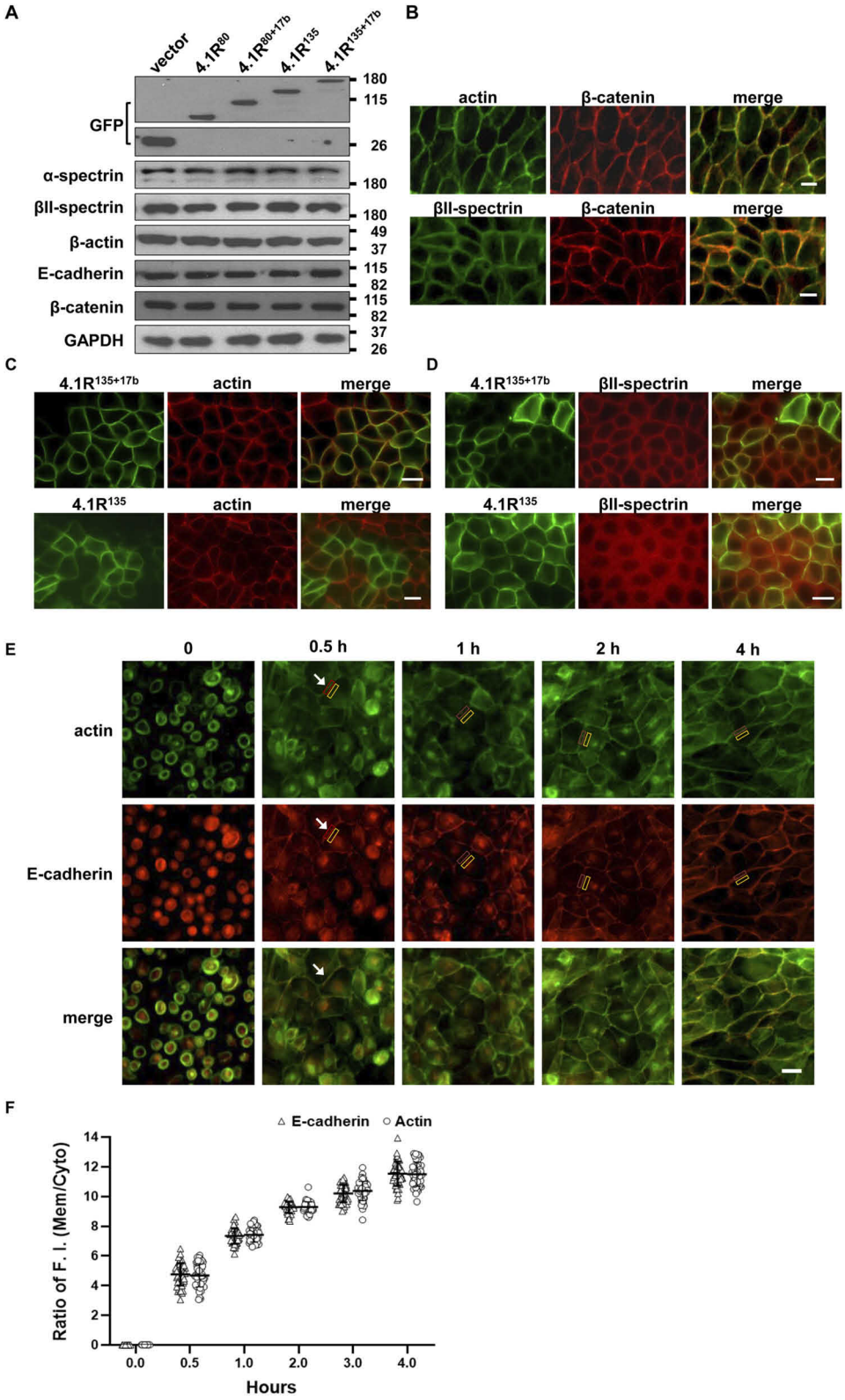

the cell–cell contacts resulted in reduced cell–cell organization of actin filaments and impaired recruitment of βII-spectrin to the AJs. These results suggest that 4.1R^{+17b} forms are critical for the membrane–cytoskeleton interface in AJs.

It has been shown that β-actin filaments are selectively enriched and associated with newly-assembled and mature AJs (55). Down-regulation of cytoplasmic actin attenuates reassembly of the peri-junctional actomyosin belt and negatively affects AJ biogenesis (55). We thus examined the behavior of actin during the reassembly of AJs in relation to that of E-cadherin during calcium-switch assays. Both actin and E-cadherin were recruited to the cell–cell contacts within 0.5 h and completely reassembled at the AJ 2 h after calcium repletion (Fig. 7*E*). The extent of E-cadherin and actin localization to cell–cell contact during the AJ reassembly process was quantified by measuring the fluorescence intensity between cell–cell contacts and the cytoplasm for each protein from the same frame. The ratio of fluorescence intensity (cell–cell contacts *versus* cytoplasm) for each protein at each time point during calcium switch was calculated from 50 cells (Fig. 7*F*). These results confirm that actin and E-cadherin are recruited to the cell–cell contact at similar rates during the AJ assembly process. Overexpression of 4.1R^{-17b} forms reduced the cell–cell contact localization of β-actin (Fig. 7*C*). The interaction of 4.1R with actin through the exon 17b region thus appears to be important for the reassembly and integrity of AJs.

4.1R^{+17b} forms a complex with fodrin and promotes fodrin–actin–4.1R ternary complex formation in the absence of exon 16

We asked whether 4.1R^{+17b} forms can associate *in vivo* with fodrin and actin in co-immunoprecipitation assays. MDCK cell extracts were precipitated with anti-actin, anti-α-spectrin, anti-ex17b, or control MIgG and RIgG Abs and examined for the presence of precipitated proteins with its respective Abs. β-Actin was identified in anti-β-actin, anti-α-spectrin, and anti-ex17b precipitates. Anti-α-spectrin antibody detected an ~240-kDa protein and a smaller ~150-kDa protein, which correspond to an intact and a degraded α-spectrin form, respectively. An ~160- and ~100-kDa 4.1R isoform were readily detected in both anti-actin and anti-α-spectrin immunoprecipitates (Fig. 8*A*, *left*). Additionally, an anti-βII-spectrin Ab detected an ~280-kDa βII-spectrin in anti-actin, anti-βII-spectrin, and anti-exon 17b precipitates (Fig. 8*A*, *right*). No immunoreactive band was detected in MIgG or RIgG precipitates (Fig. 8*A*). Collectively, these findings suggest that exon 17b-containing 4.1R isoforms occur *in vivo* in a supramolecular complex with α- and βII-spectrin tetramers and actin filaments.

The association of 17b-containing forms with spectrin–actin in a complex prompted us to inquire whether exon 17b could stimulate the fodrin–actin–4.1R ternary complex formation in the absence of exon 16. We generated various GST–4.1R–exon 16–17−17b recombinant peptides that carried distinct combinations of the alternatively-spliced exons 16–17−17b (Fig. 8, *B* and *C*), and their ability to promote fodrin/actin association was tested in co-sedimentation assays (Fig. 8*D*). As noted in an earlier report (36), ~55–65% of fodrin remained in the supernatant when fodrin and actin were sedimented without the addition of 4.1R. 4.1R–SAB peptides (Ex16/17) carried the alternatively-spliced exon 16 along with the constitutive exon 17–sedimented fodrin to the pellet fraction with only ~10% remaining in the supernatant. When exon 16 was omitted (Ex17), ~65% of fodrin was detected in the supernatant and 35% in the pellet fraction. The inclusion of exon 17b in the absence of exon 16 (Ex17/17b) resulted in a shift of ~90% fodrin from the supernatant to the pellet. Thus, exon 17b–encoded peptides behaved similarly to that of exon 16 and stimulated co-sedimentation of fodrin and F-actin. It is interesting to note that exon 17 (Ex17b) also contributed to the sedimentation of fodrin and actin as its absence suppressed the binding (Fig. 8*D*). Altogether, these results show that sequences carried by exon 17 in conjunction with either exon 16 or exon 17b are necessary and sufficient to stimulate fodrin/actin association. A graphic presentation of the percentage of pelleted fodrin following stimulation with the various 4.1R-exon 16–17−17b peptides is shown in Fig. 8*E*.

Depletion of 4.1R^{+17b} forms affects the organization of spectrin–actin cytoskeleton and attenuates the initial recruitment of E-cadherin to the AJs

To ensure physiological relevance of the results obtained from overexpression of 4.1R^{+17b} or 4.1R^{-17b} forms, we further analyzed the effects of 4.1R^{+17b} silencing and its rescue on the dynamics of epithelial AJs using the inducible Tet-On shRNA knockdown or transfection of siRNA.

MDCK Tet-On stable lines with a control shRNA or exon 17b shRNA in pTRIPZ were generated. Red fluorescent protein (RFP) served as an expression marker. 4.1R^{+17b} knockdown and rescue were validated in immunofluorescence staining and

Figure 7. Expression of 4.1R^{+17b} or 4.1R^{-17b} forms does not impede the protein levels of AJ and spectrin–actin cytoskeleton, but 4.1R^{-17b} expression affects the organization of the spectrin lattice in the area of cell–cell contacts. MDCK cells transfected with EGFP–4.1R^{+17b} or EGFP–4.1R^{-17b} forms were analyzed for AJ and spectrin–actin protein levels as well as for the intracellular localization of actin and βII-spectrin 36 h post-transfection. *A*, Western blotting analyses for AJ and actin skeleton proteins from MDCK cells transfected with EGFP–4.1R^{80}, EGFP–4.1R^{80+17b}, EGFP–4.1R^{135}, or EGFP–4.1R$^{135+17b}$. Equal amounts of lysates from each transfected culture were immunoblotted with anti-GFP, α-spectrin, βII-spectrin, β-actin, E-cadherin, or β-catenin Ab. GAPDH served as a loading control. Molecular mass markers (*kDa*) are provided. *B*, F-actin and βII-spectrin co-localize with β-catenin at the AJs of MDCK cells. MDCK were plated on coverslips and stained with Alexa Fluor 488 phalloidin for actin or anti-βII-spectrin Ab for βII-spectrin. Both were dual-immunolabeled for β-catenin and revealed with a Zeiss microscope. *Bar*, 10 μm. *C*, reduction of actin at AJs of EGFP–4.1R^{135}–expressing cells but not that of EGFP–4.1R$^{135+17b}$–expressing cells. MDCK cells transfected with EGFP–4.1R$^{135+17b}$ or EGFP–4.1R^{135} were labeled with Alexa Fluor 568 phalloidin for actin. *D*, EGFP–4.1R^{135} but not EGFP–4.1R$^{135+17b}$ expression transforms junctional localization of βII-spectrin into diffuse cytoplasmic accumulation. MDCK cells transfected with EGFP–4.1R$^{135+17b}$ or EGFP–4.1R^{135} were labeled for the presence of βII-spectrin. *Bar,* 10 μm. *E*, presence of actin at the cell–cell contacts coincides with that of E-cadherin during the AJ reassembly process. MDCK cells were stained for actin and E-cadherin at the indicated time after calcium repletion. Note: fluorescence labeling shows formation of the circumferential F-actin and E-cadherin at the AJs after 0.5 h of calcium repletion (*arrows*) and persists through the AJ maturation process. *Bar*, 10 μm. *F*, ratio of the fluorescence intensity of E-cadherin and actin at the cell–cell junction (*red boxed region* of *panel E*) *versus* adjacent cytoplasm (*yellow boxed region* of *panel E*) was measured ($n = 50$). (*F.I.*, fluorescence intensity; *Mem,* membrane; *Cyto*, cytoplasm). Values are mean ± S.E.

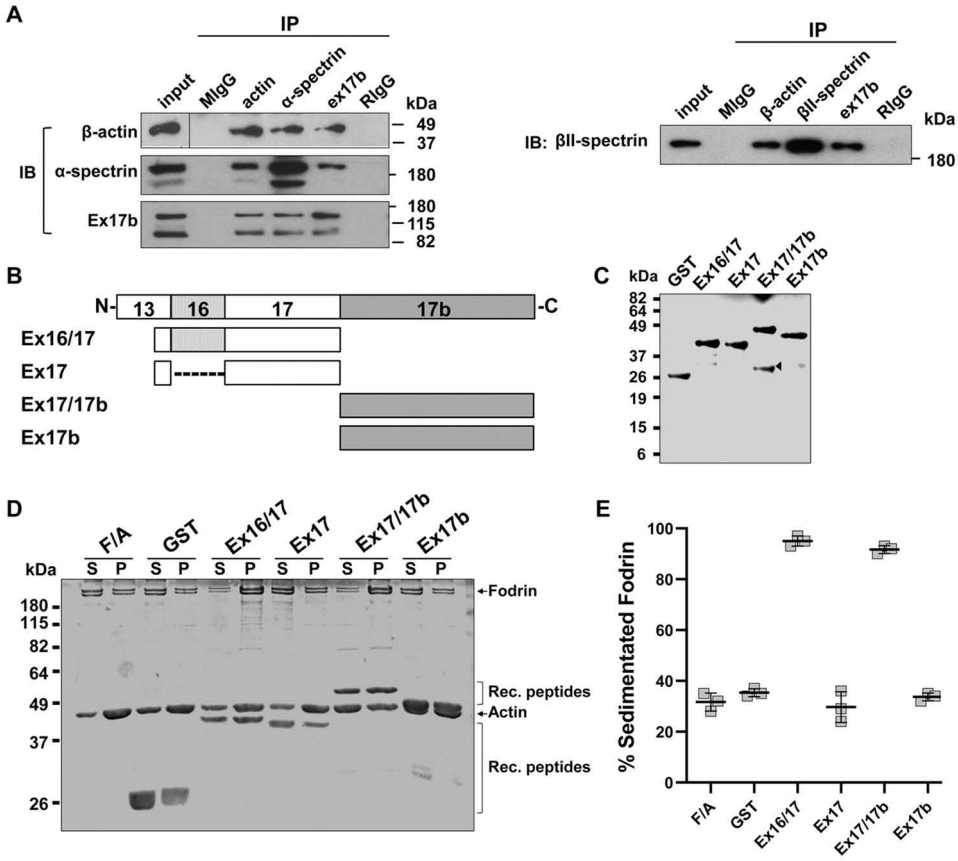

Figure 8. 4.1R forms carrying exon 17b associate with spectrin and actin and induce fordin–actin–4.1R ternary complex formation. *A*, association of endogenous 17b-containing 4.1R forms, actin, and spectrin was analyzed in an immunoprecipitation assay. *Left*, MDCK cell lysates were immunoprecipitated with a control MIgG, anti-β-actin, anti-α-spectrin, anti-ex17b Ab, or a control RIgG and examined with their respective antibodies for the presence of the precipitated protein. *Right,* MDCK lysates precipitated with MIgG, anti-β-actin, anti-βII-spectrin, anti-ex17b Ab, or RIgG and immunoblotted with an anti-βII-spectrin Ab for its presence in each precipitate. Molecular mass markers (*kDa*) are provided. *B*, schematic diagram of GST–4.1R–exon 16–17−17b constructs carrying various exon compositions used for the sedimentation assays. *C*, Coomassie Blue-stained gel of bacterially-expressed GST fusion proteins of different combinations of exon 16–17−17b peptides. *Arrowhead,* degradation product in purified GST–Ex17/17b fusion. Molecular mass markers (kDa) are provided. *D*, co-sedimentation assays using GST–4.1R peptides, rat brain fodrin, and F-actin followed by separation of supernatant (*S*) and pellet (*P*) fractions by ultracentrifugation and analysis by SDS-PAGE. Three independent experiments were performed. *E*, graphic presentation of the results obtained in D using National Institutes of Health Image software for quantitation of the fodrin band present in the pellet fraction.

immunoblot assays. In the absence of doxycycline, no RFP^+ cells were detected in 17b shRNA cells and they had nearly equal 17b intensity at the cell–cell contacts (Fig. 9*A*, *−dox*). In the presence of doxycycline, significantly decreased exon 17b signals were found at the cell–cell contacts of the RFP^+ cells but not that of RFP^- cells (Fig. 9*A*, *+dox*). Co-expression of a $4.1R^{135+17b}$ rescue construct resulted in the reappearance of the 17b signal at the cell borders of the RFP^+ cells (Fig. 9*A*, *+dox 4.1Rres*). $4.1R^{+17b}$ protein was effectively knocked down by greater than 95% in 17b shRNA cells in the presence of doxycycline (Fig. 9*B*). $4.1R^{+17b}$ rescue constructs expressed almost the same amount as that of the endogenous forms (Fig. 9*B*). When the AJ and spectrin/actin cytoskeleton proteins were examined, $4.1R^{+17b}$ depletion and rescue did not affect the supply of the AJ and actin cytoskeletal proteins, as no significant differences in E-cadherin, β-catenin, α- and βII-spectrin, and β-actin levels were observed (Fig. 9*B*).

We next analyzed whether $4.1R^{+17b}$ depletion had any effect on F-actin and βII-spectrin localization. Evaluating the actin fluorescence at cell–cell contacts of a mix of RFP^- and RFP^+ populations showed strong actin staining in RFP^- and RFP^- cell contacts, whereas a reduction of actin signal occurred at the shared RFP^- and RFP^+ cell borders (Fig. 9*C*, *upper panel*). Intensity was notably reduced when both neighboring cells were depleted of $4.1R^{+17b}$ in the RFP^+ cell borders (Fig. 9*C*, *upper panel*). Actin signal reappeared to the full extent at the cell borders of RFP^+ cells when $4.1R^{135+17b}$ rescue construct was expressed in the knockdown cells (Fig. 9*C*, *upper panel*). The cell–cell junctions marked by βII-spectrin staining were different in RFP^- and RFP^+ cell borders. In RFP^- cells, there was no obvious cytoplasmic localization of βII-spectrin; intercellular contacts exhibited normal βII-spectrin staining (Fig. 9*C*, *lower panel*). In RFP^+ cells, βII-spectrin largely diffused throughout the cytoplasmic compartment with no distinguishable junctional staining (Fig. 9*C*, *lower panel*). $4.1R^{135+17b}$ rescue restored the cell–cell contact localization of βII-spectrin in RFP^+ cells (Fig. 9*C*, *lower panel*). These results confirm the overexpression data (Fig. 7, *C* and *D*) and suggest an important role of $4.1R^{+17b}$ forms in the junctional organization of the actin–spectrin cytoskeleton.

We examined whether the altered actin and βII-spectrin localization occurring in response to $4.1R^{+17b}$ depletion impacted the reassembly of AJs. MDCK transfected with a control siRNA or an ex17b-specific siRNA in the absence or pres-

ence of a $4.1R^{135+17b}$ rescue construct was used for these studies. The control siRNA cells expressed both 160- and 100-kDa 4.1R, whereas the exon 17b-siRNA sample reduced the 160 kDa to almost 0% and the 100 kDa by greater than 90% as assessed with an anti-ex17b antibody (Fig. 9*D*). The rescue construct $4.1R^{135+17b}$ was thus effectively expressed in siRNA-treated cells (Fig. 9*D*).

In calcium-switch assays, E-cadherin disengaged from the cell–cell contacts and became internalized in all treatments at 0 h (Fig. 9*E*, *Ctrl*). In control cells, E-cadherin started to appear at the cell–cell contacts of some cells 0.5 h after calcium replenishment, and the number of cells with E-cadherin at the cell–cell contacts increased substantially 1 h after calcium replenishment. Finally, E-cadherin appeared at the cell–cell contacts of

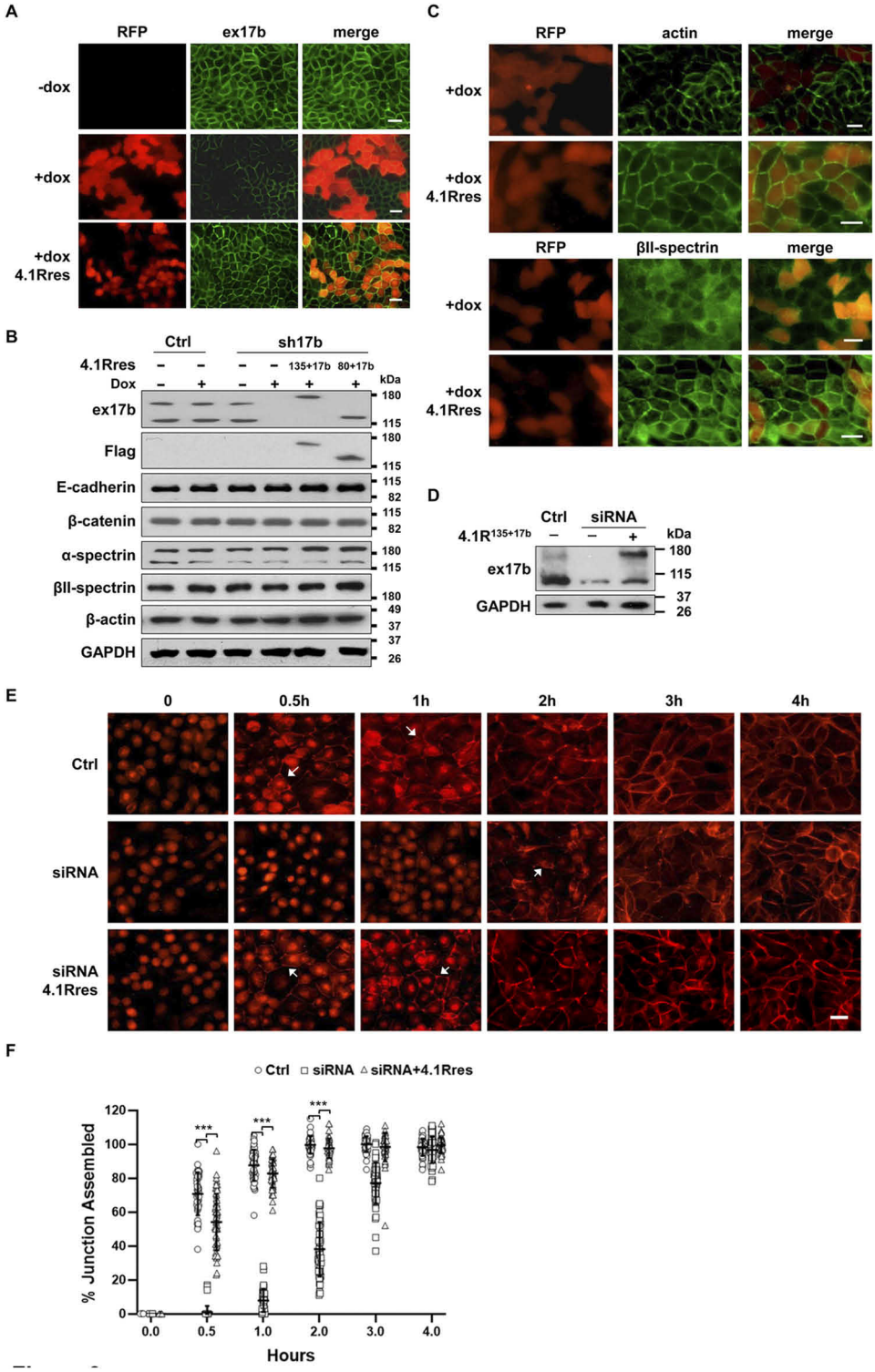

the majority of cells after 2 h, and exclusively localized at the cell–cell contacts of all cells by 3 h after calcium was replenished (Fig. 9*E*, *Ctrl*). In ex17b–siRNA cells, the first appearance of E-cadherin at the cell–cell contacts was observed 2 h after calcium replenishment, an ~1.5-h delay when compared with that of the control cells (Fig. 9*E*, *siRNA*). E-cadherin appeared at the cell–cell contacts of many more ex17b–siRNA cells by 3 h and on the majority of the cells 4 h after calcium replenishment (Fig. 9*E*, *siRNA*). The ex17b–siRNA with 4.1R$^{135+17b}$-rescued cells behaved similarly to that of the control cells with the reappearance of E-cadherin at 0.5 h and proceeded to localize at the cell–cell contacts of all cells 3 h after calcium replenishment (Fig. 9*E*, *siRNA 4.1Rres*).

Quantification analyses of the percentage of junction assembled during the time courses after calcium replenishment was measured by the ratio of the E-cadherin–labeled length *versus* the length of the cell periphery from 50 cells with its respective treatment (Fig. 9*F*). At 0.5 and 1–4 h after calcium replenishment, the junctions assembled in each treatment were as follows: ~70, 87, 99, 100, and 98% in control cells; ~0.9, 8.1, 38, 77, and 96% in siRNA knockdown cells; and ~53, 83, 97, 98, and 99% in rescue cells. A drastic reduction of E-cadherin at 0.5, 1, and 2 h after calcium replenishment in 4.1R siRNA knockdown was noted when compared with that of control and rescue cells. However, the siRNA knockdown cells reached a delayed percentage of junctions assembled after 3 h of calcium replacement that was nearly as high as control (Fig. 9*F*).

Like 4.1R^{80}- and 4.1R^{135}-expressing cells, ex17b–siRNA-depleted cells reduced E-cadherin intensity at the cell–cell contacts at the initial reassembly 0.5 and 1 h after replenishment with normal calcium medium. In contrast to that of 4.1R^{80}- and 4.1R^{135}-expressing cells where there is a persistent lack of E-cadherin at the cell–cell contacts throughout the reassembly of AJs, the ex17b–siRNA knockdown cells eventually exhibited E-cadherin recruitment to the cell–cell contacts (after 3 h). The occupancy of EGFP–4.1R^{-17b} at the cell–cell contacts of the overexpressing cells but not that of ex17b–siRNA knockdown cells may play a role in such discrepancy. Nonetheless, the critical role for 4.1R^{+17b} forms in AJ assembly seems to be at the initial junctional formation when actin also participates in the assembly process (Fig. 7*E*). Together, these results show that 4.1R^{+17b} is important for the formation of normal apical AJs in the MDCK cell monolayer.

Discussion

Interplay between the peri-junctional F-actin cytoskeleton and the plasma membrane is essential for the integrity and remodeling of epithelial AJs during normal epithelial morphogenesis. Disruption of this interplay causes pathological abnormalities. Finding the components that link epithelial junctions and the actin cytoskeleton will improve our understanding of the regulation of AJs. 4.1R has been implicated in linking the AJ (38) complex to the cytoskeleton. However, the precise 4.1R isoform(s) participating, and the mechanisms involved in junctional stability or remodeling, remained unclear prior to this study. Our results offer the first direct evidence that epithelial-specific 4.1R^{+17b} forms are key molecular constituents of the membrane skeleton involved in regulating AJs. 4.1R^{+17b} isoforms are exclusively co-localized and associated with the AJ proteins. The membrane-binding domain of 4.1R links to the armadillo repeats 1 and 2 of β-catenin, whereas exon 17b–encoded peptides interact with actin and form a spectrin–actin–4.1R ternary complex. Lack of 4.1R^{+17b} isoforms significantly attenuated initial calcium-dependent AJ assembly, and its re-expression restored AJ junctional dynamics. The effects of 4.1R^{+17b} on epithelial junctions are likely mediated by recruitment and/or stabilization of β-catenin and the spectrin–actin cytoskeleton to the areas of cell–cell contact.

Some 4.1R isoforms serve as adapters that link the actin-based cytoskeleton to plasma membrane proteins (29, 34–36). Exon 16 of 4.1R is vital for the stabilization of the spectrin–actin complex in the red blood cell cytoskeleton (34, 35) and modulates the membrane mechanical properties of neuronal cells (36). However, exon 17b-containing 4.1R^{+17b} isoforms are the predominant forms expressed in confluent MDCK cells. Our results show that an inverse reciprocal expression of decreased exon 16 and increased exon 17b occurs during confluence of MDCK. Exon 17b–encoded peptide interacted with β-actin and formed 4.1R–fodrin–actin ternary complexes in the absence of exon 16. The binding properties of exon 17b thus appear to compensate for the lack of exon 16 in promoting fodrin/actin associations in epithelial cells. Examination of

Figure 9. Down-regulation of 4.1R^{+17b} expression affects the organization of the spectrin–actin skeleton at cell–cell contacts and attenuates the initial reassembly of E-cadherin at the AJs. *A–C,* MDCK Tet-On stable lines were generated with a control scramble shRNA (*Ctrl*) or 4.1R-exon 17b shRNA (*sh17b*) in pTRIPZ where RFP served as an expression marker. sh17b lines grown in the absence (−*dox*) or presence (+*dox*) of doxycycline (*dox*) and sh17b line co-expressing rescue construct 4.1R$^{135+17b}$ grown in the presence of doxycycline (+*dox 4.1Rres*) were analyzed. *A*, 4.1R^{+17b} is silenced at the intercellular junctions, and 4.1R$^{135+17b}$ rescue restores its expression at the cell–cell contacts. sh17b lines with indicated treatments were immunofluorescently-stained with an anti-ex17b antibody and revealed with a Zeiss microscope. *Bar*, 10 μm. *B*, 4.1R^{+17b} silence and rescue do not affect the protein levels of the AJs and spectrin–actin cytoskeleton. Western blotting of cell lysates from control and sh17b cell lines treated as indicated were analyzed for ex17b, 4.1R rescue forms (*Flag*), E-cadherin, β-catenin, α-spectrin, βII-spectrin, and β-actin with its respective antibody. GAPDH served as a loading control. Molecular mass markers (kDa) are provided. *C*, immunofluorescence staining for actin and βII-spectrin in sh17b cells treated as indicated (+*dox* and +*dox 4.1Rres*) and revealed with a Zeiss microscope. *Upper panel*, depletion of 4.1R^{+17b} forms results in the reduction of actin at the AJs, and 4.1R$^{135+17b}$ expression restores cell–cell contact localization of actin. *Lower panel,* βII-spectrin in 4.1R^{+17b}-depleted cells largely distribute in the cytoplasmic compartment, and 4.1R$^{135+17b}$ expression restores cell–cell contact localization of βII-spectrin. *Bar,* 10 μm. *D* and *E*, 4.1R^{+17b} knockdown was achieved by exon 17b-specific siRNA (*siRNA*), and rescue was accomplished by co-expression rescue construct 4.1R$^{135+17b}$ (*siRNA 4.1Rres*). A scramble nontargeting siRNA served as a control (*Ctrl*). *D*, siRNA-mediated knockdown of 4.1R^{+17b} forms reduces 4.1R$^{135+17b}$ and 4.1R^{80+17b} expression, and rescue construct restores 4.1R$^{135+17b}$ expression in MDCK. Cell lysates from MDCK with indicated treatments were analyzed with an anti-ex17b antibody. GAPDH served as a loading control. Molecular mass markers (*kDa*) are provided. *E*, knockdown of 4.1R^{+17b} forms delays the initial recruitment of E-cadherin to cell–cell contacts, and 4.1R$^{135+17b}$ expression restores the normal reassembly process. MDCK cells treated as indicated and subjected to calcium switch were immunofluorescently-stained for E-cadherin. Note: E-cadherin localizes at cell peripheries at early time points (0.5 and 1 h) in both control and rescue cells but not in ex17b–siRNA knockdown cells. E-cadherin recruits to cell border of all treatments 4 h after calcium repletion. *Bar,* 10 μm. *F*, quantification of percent of junction assembly after calcium switch. Data are shown as mean ± S.E. of 50 cells. *Asterisks* indicate statistical significance (***, $p < 0.001$).

actin-binding motifs shows a sequence similarity between amino acids 94–118 (ALKFSVSPASSQRQLGEKKAESSEE) of exon 17b and known actin-binding sites on the Carcinoembryonic Antigen Cell Adhesion Molecule 1 (CEACAM1) (56), caldesmon (57), myosin II (58), and villin (59). Whether this exon 17b sequence or a different motif within it is responsible for interaction with actin is under investigation.

We studied the contribution of $4.1R^{+17b}$ forms to mature AJs by expressing $4.1R^{-17b}$ or depleting $4.1R^{+17b}$ forms in MDCK cells. Both resulted in impaired F-actin cytoskeleton organization similar to that of 4.1R gene knockout in mouse gastric epithelia (38). E-cadherin signal is reduced at the AJs in this study, whereas the weakened attachment of E-cadherin to cytoskeleton is identified in the previous report (38). In contrast to the earlier report, we observed no significant differences in β-catenin protein level and localization at the AJs in the presence or absence of $4.1R^{+17b}$ forms. Whether the discrepancy is due to difference between the gastric and renal epithelia remains to be further examined.

The prior study of 4.1R in epithelial AJs *in situ* (38) revealed a possible role of 4.1R in epithelial biology; however, that *in situ* analysis does not allow for examination of the mechanisms involved in junctional stability or remodeling. We explored the participation of $4.1R^{+17b}$ forms in the regulation of the dynamics of AJs induced by calcium switch in MDCK cells expressing $4.1R^{-17b}$ forms or knockdown $4.1R^{+17b}$ forms. E-cadherin was delayed in its participation in the initial reassembly of AJs in both EGFP–$4.1R^{80}$–expressing and ex17b–siRNA knockdown cells. It ultimately associated with the AJ in exon 17b knockdown cells, but was almost absent at the cell–cell contacts in EGFP–$4.1R^{80}$–expressing cells throughout the reassembly process. This difference might be because the 4.1R paralogues 4.1G, 4.1B, and 4.1N are also expressed in epithelia (60). Both 4.1R and 4.1N are localized at the lateral membrane of epithelial cells (60). The MBD, SAB, and CTD are highly-conserved among 4.1 family members. We speculate that the function of $4.1R^{+17b}$ at the AJs might be replaceable by redundancy among other 4.1 family members. In the overexpression studies, the occupation of EGFP–$4.1R^{80}$ at the cell–cell contacts may prevent the recruitment of 4.1R paralogues to the sites. In contrast, the knocked down cells would have sites available for paralogue binding. This may also explain why 4.1R homozygous knockout mice are viable (61) despite the evidence from the earlier report (38) and current studies that 4.1R is involved in the assembly and stabilization of AJs in the epithelial integrity. Whether any of these family members might compensate is under further investigation.

Recent studies have emphasized the importance of the association between epithelial junctions and the membrane skeleton in AJ assembly. Adducin mediates spectrin–actin interactions and links the complex to the membrane (26). Depletion of adducin significantly attenuated calcium-dependent AJ assembly. Ankyrin-G provides a direct link between E-cadherin and the spectrin/actin cytoskeleton by recruiting βII-spectrin to E-cadherin–β-catenin complexes (27). E-cadherin requires both ankyrin-G and βII-spectrin for its cellular localization as depletion of either ankyrin-G or βII-spectrin blocks the accumulation of E-cadherin at sites of cell–cell contacts. Spectrin is also a major component of the erythrocyte cytoskeleton. 4.1R binds to spectrin (62) and promotes the binding to actin (63). These components play an essential role in the maintenance of the mechanical stability and shape of the cell membrane. Depletion of $4.1R^{+17b}$ diminishes junctional recruitment of βII-spectrin, reduces peri-junctional actin bundles, and prevents the assembly of E-cadherin at cell–cell contacts. Like the spectrin–adducin–ankyrin complex, the spectrin–$4.1R^{+17b}$-based membrane cytoskeleton complex may also be needed for AJ integrity and remodeling. Additional studies in a system that investigates the behavior of the actin–spectrin-based membrane association with 4.1R and the effects of actin and spectrin manipulations in AJ assembly would be needed to provide mechanistic insight into how 4.1R organizes the actin or spectrin cytoskeleton.

We reported earlier that 4.1R localizes at the TJ and associates with ZO-2 through the CTD domain (37). The specific 4.1R isoform(s) in TJs have not been characterized. AJ assembly is known to be a prerequisite for subsequent formation of TJs (3). The impairment of AJ establishment in the absence of $4.1R^{+17b}$ forms most likely attenuates TJ assembly. It will be of interest to discern the precise 4.1R form(s) in TJs and to compare the functional differences between 4.1R forms in the TJs and AJs.

The splicing switch involving the exclusion of exon 16 and inclusion of exon 17b of 4.1R coincides with nuclear to cell–cell contact localization and cell density–dependent growth arrest of epithelial cells. It is known that cooperation between two motifs in exons 5 and 16 are required for the nuclear location of 4.1R in proliferating cells (64). Because exon 5 is included in nearly all isoforms in MDCK cells, the shift in localization in confluent cells is at least partly accomplished by isoform switch from exon 16 inclusion to exclusion in confluent cells. Regulated alternative splicing thus plays a critical role in mediating temporal and/or spatial splicing decisions of 4.1R during maturation of epithelial cells. Multiple *cis*- and *trans*-acting factors have been shown to regulate exon 16 expression (50, 65). In contrast, the control of exon 17b inclusion has not been characterized. It would be of interest to know whether an epithelial-specific splicing factor is involved in exon 17b expression and how the coordinated splicing regulation between exon 16 exclusion and exon 17b inclusion is mediated during differentiation.

Protein 4.1R is a member of the FERM protein family. The FERM domain is a common protein module involved in localizing proteins to the plasma membrane where they function as membrane–cytoskeletal linkers and regulators of multiple signaling pathways (66, 67). Some members of this family have also been implicated in tumor progression (68). 4.1R was found to be involved in meningioma pathogenesis (69) and ependymal tumors (70). Despite extensive research on 4.1R's role as a tumor suppressor, the mechanism by which 4.1R suppresses tumorigenesis has remained elusive. The NF2 tumor suppressor merlin is a critical suppressor of meningiomas and schwannomas (71). It is absent in virtually all schwannomas, and many meningiomas and ependymomas (72, 73). Merlin physically interacts with and stabilizes actin filaments *in vitro* (74) and interacts with βII-spectrin (31). The direct involvement of merlin in actin–cytoskeleton organization suggests that alterations

in the cytoskeleton are an early event in the pathogenesis of some tumor types (31). Interestingly, merlin also localizes to AJs and associates with AJ components (75). Merlin controls AJ assembly and contact-dependent growth inhibition directly from sites of cell–cell contact. Its deficiency promotes tumorigenesis and metastasis by destabilizing AJs (30). It is tempting to speculate that 4.1R functions as a tumor suppressor in a similar manner.

In summary, this study demonstrates that $4.1R^{+17b}$ stabilizes the AJs by linking the cytoskeleton to the membrane. This in turn impacts the process of assembly and disassembly of AJs. Further elucidation of the underlying mechanisms should provide important insights into the regulation of epithelial AJ remodeling and biological role of 4.1R.

Experimental procedures

Plasmid constructs

All DNA constructs were made using standard cloning procedures and confirmed by sequencing. 4.1R mini-cDNA libraries were amplified from MDCK RNA using oligo(dT) for RT, and the antisense primer located at the end of coding sequences (D4.1R-21K-As, 5′-TTGGTACCTCATTCCTCAGAGATTTCAGTCTCCTGA-3′) (GenBank™ accession number NM_001003362.1) and the sense primer 1A (D4.1R-Ex1A-S, 5′-TGGCAGGAACCTCTTAAAGGGCGAGA-3′); 1B (D4.1R-Ex1B-S, 5′-ATGTGTCCCTGTGATGGCTCCACGGCTTCT-3′), or 1C (D4.1R-Ex1C-S, 5′-CCTTCTCCTGCCATTGTTCCTCG-3′) (GenBank™ accession number NC_006584.3) for PCR. The products were cloned into TOPO-TA vector (Invitrogen). Approximately 100 4.1R clones positive for the constitutive exon 13 from each group were transferred to Hybond N+ membranes and then probed for alternative spliced exons (exon 5, 14, 15, 16, 17a, 17b, 18, and 19) using DIG nucleic acid detection kit (Roche Applied Science). The identified representative species of 4.1R isoforms were subsequently cloned in-frame with EGFP into pEGFP-C1 (Clontech) or pcDNA3.1(+)-3Flag (76).

The 135-kDa (1–862 aa), 80-kDa (210–862 aa), HP (1–209 aa), MBD (210–507 aa), 16-kDa (508–614 aa), SAB (615–714 aa), and CTD (715–862 aa) of 4.1R (GenBank™ accession number NM_001166005.1) were amplified from HUVEC and cloned into pGEX-6P1 vector (Amersham). The GST–4.1R–SAB with or without exon 16 was amplified from pGEX-2T-10kd(−/−/+) or 10kd(−/−/−) (36) and subcloned into pGEX-6P1 to form Ex16/17/GST and Ex17/GST, respectively. Ex17/17b or Ex17b was cloned into pGEX-6p1 using primers D4.1R-17-S (5′-CGGAATTCGATTTAGACAAAAGTCAAGAAGAGA-3′) or D4.1R−17b-S (5′-CACCCTCATTCGAAGTTTCCAGGTCGACAA-3′) and D4.1R−17b-As (5′-TTGTCGACCTGGAAACTTCGAATGAGGGTG-3′) for Ex17/17b/GST and Ex17b/GST, respectively. The full-length first 100 amino acids or the last 100 amino acids of exon 17b were cloned into yeast two-hybrid Gal4 DNA-BD vector pGBKT7 (Clontech) for yeast two-hybrid assays. Similarly, the MBD domain of 4.1R was cloned into pGBKT7 for its interaction with the armadillo repeats cloned into Gal4 DNA-AD vector pGADT7.

The full-length (1–781 aa), NTD (1–140 aa), armadillo domain (141–664 aa), and CTD (665–781 aa) of β-catenin (GenBank™ accession number NM_001137652.1) were amplified from HUVEC and cloned into pCl-neo vector (Promega) to generate CTNNB-FL/pCl-neo, CTNNB-NTD/pCl-neo, CTNNB-ARM/pCl-neo, and CTNNB-CTD/pCl-neo for *in vitro* transcription and translation. The full-length armadillo domain or its repeat deletions were cloned into pGADT7 fused with Gal4 DNA-AD to produce 1–12/pGADT7, 1–10/pGADT7, 1–8/pGADT7, 1–4/pGADT7, 1–2/pGADT7, 3–12/pGADT7, and 5–12/pGADT7 for yeast two-hybrid assays.

Exon 17b shRNA with the targeted nucleotide sequences CCTGTCGGAGTCTCCACAAAG (sh121) were cloned into pTRIPZ lentiviral shRNAmir vector (Open Biosystems) to form pTRIPZ-$4.1R^{ex17b}$ shRNA. Packaging, transduction, and induction of pTRIPZ shRNAmir are as described in the manufacturer's instructions. 4.1R rescue plasmids were constructed in the Tet-On inducible expression vector pTRIPO, in which the AgeI–MluI fragment of pTRIPZ (containing the TurboRFP tag and the 5′mir30/3′mir30 sequences) was replaced by an AgeI–HpaI–XhoI–EcoRI–MluI polylinker sequence. Establishment of the inducible pTRIPO-3Flag-$4.1R^{160res}$ and pTRIPO-3Flag-$4.1R^{100res}$ was constructed by two-step cloning: pcDNA3.1–3Flag-$4.1R^{160res}$ and pcDNA3.1–3Flag-$4.1R^{100res}$ with the underlined mutations at the shRNA target sequences (CCTGTCGGAATCTCCGCAAAG). These were incorporated into pcDNA3.1–3Flag-4.1R and subsequently cloned into pTRIPO.

RT-PCR analyses

RT-PCR analysis of exon 16 and exon 17b expression was performed using a limiting cycle amplification protocol that obtains the PCR product within its linear range (50). RNAs from nonconfluent, sub-confluent, and confluent MDCK cells were reverse-transcribed using the oligo(dT) primer. PCRs were performed with Ex13-S (5′-AGAGCCCACAGAAGTGTGGA-3′) and Ex17-As (5′-AGCTCACTGATGCTGGCATGAT-3′) for exon 16 and with Ex17-S (5′-AATGGGCAGCTTCCCACAGGA-3′) and Ex18-As (5′-GTTTGAGTCTTCACCAGGGGA-3′) for exon 17b. PCR products were fractionated on 2% agarose gels or 5% DNA polyacrylamide gels and quantified using analytic software from a ChemiImager™ 5500 System (Alpha Innotech Co.). Two samples were performed with each confluent stage in each experiment. Each experiment was repeated three times. Averages and standard deviations (S.D.) were calculated from three independent experiments ($n = 3$). E16 or E17b inclusions were calculated as the percent of exon 16 inclusion (+E16)/total products (set as 100%) or exon 17b inclusion (+E17b)/total products in individual lanes.

Cell culture and induction of junctional remodeling

MDCK II provided by Drs. Alan Fanning and James Anderson (University of North Carolina, Chapel Hill) were grown in Dulbecco's modified Eagle's medium supplemented with 10% heat-inactivated fetal bovine serum (Sigma), penicillin (50 μg/ml), and streptomycin (50 μg/ml). MDCK cells were plated on glass coverslips at three different densities. The density of confluent cells was 10 times higher than that of sub-confluent cells and 50 times higher than that of nonconfluent cells. To study the formation of epithelial AJs, confluent MDCK monolayers were first depolarized by overnight incubation in low-

calcium medium (calcium-free Eagle's minimal essential medium and 2% dialyzed fetal bovine serum, pH 7.4). To induce junctional reassembly, the cells were returned to normal cell culture media with 1.8 mM calcium concentration for the indicated times (referred to hereafter as "calcium repletion").

MDCK cells were transduced with pTRIPZ-4.1R^{ex17b} shRNA or control scramble shRNA and selected for stable cell lines with puromycin. shRNA expression was induced with 200 ng/ml doxycycline where RFP served as an shRNA expression marker. To rescue 4.1R^{+17b} expression in knockdown cells, pTRIPZ-4.1R^{ex17b} shRNA MDCK was either transfected with pcDNA3.1–3Flag-4.1R^{160res} and pcDNA3.1–3Flag-4.1R^{100res} or transduced with inducible lentiviral pTRIPO-4.1R^{160res} and pTRIPO-4.1R^{100res} or an empty vector and selected for stable lines. 4.1R^{160res} or 4.1R^{100res} expression was induced in the presence of doxycycline in growth medium.

Co-immunoprecipitation and immunoblotting

Co-immunoprecipitation of 4.1R and adherens junction proteins was performed using MDCK cell lysates. Cell lysates or immunoprecipitates were analyzed by 10 or 15% SDS-PAGE and electrotransferred onto a polyvinylidene difluoride (PVDF) (Millipore) or nitrocellulose membrane (Maine Manufacturing, LLC). The detection of 4.1R forms, β-catenin, E-cadherin, β-actin, spectrin, and GAPDH was carried out by immunoblotting with the following: anti-4.1R-HP, anti-4.1R-exon 13, anti-4.1R-exon 16, anti-4.1R-exon 17b, and anti-β-catenin (BD Transduction Laboratories); anti-E-cadherin (rr1, Developmental Studies Hybridoma Bank (DSHB)); anti-ZO1 (61-7300, Thermo Fisher Scientific); anti-β-actin (A2228, clone AC-74, Sigma); anti-spectrin α-chain (nonerythroid) (MAB 1622, Chemicon); anti-β-spectrin II (612563, BD Transduction Laboratories); and anti-GAPDH (SAB2100894, Sigma) antibody diluted in either 4% milk in TBST (20 mM Tris-HCl, pH 7.6, 140 mM NaCl, 0.1% Tween 20) or in antibody enhancer diluent (Amresco, Inc., Solon, OH), and developed using an ECL detection kit (Amersham Biosciences). The presence of exogenously expressed Flag-4.1R^{160res} and 4.1R^{100res} proteins was detected with anti-FLAG (F7425, F3165, Sigma) antibody. VeriBlot secondary antibodies (ab131366 or ab131368, Abcam) were used for co-immunoprecipitation Western blotting analyses.

Indirect immunofluorescence and imaging

For immunolabeling experiments, MDCK cells were grown on either collagen-coated permeable polycarbonate filters (0.4-μm pore size; Costar, Cambridge, MA) or on collagen- or poly-D-lysine–coated coverslips. Cells were fixed in PBS containing 4% paraformaldehyde for 15 min and then permeabilized in 0.25% Triton X-100 in PBS for 5 min at room temperature. Cells were then blocked in 10% goat serum for 30 min and exposed to primary and secondary antibodies at room temperature for 1 h each. Alexa Fluor 568 goat anti-mouse, Alexa Fluor 568 goat anti-rabbit, Alexa Fluor 488 goat anti-mouse, Alexa Fluor 488 goat anti-rabbit secondary antibody, and Alexa Fluor 488 phalloidin were obtained from Invitrogen. All samples were counterstained with 4,6-diamidino-2-phenylindole. The samples were viewed with a Zeiss Axiovert 200M inverted microscope or a Zeiss Axio Imager.Z1 microscope (Zeiss, Inc.). The images were collected using SlideBook^{TM} 4.0 or AxioVision Rel. 4.8 software and processed using Photoshop software (Adobe Systems, Inc.).

Quantification of junction assembly during the calcium switch was carried out with ImageJ software as described (77). In brief, the outline of the cell was drawn as the length of the cell periphery, and the regions of cell–cell contact labeled by E-cadherin were drawn as the labeled length. Five EGFP^{+} cells/field (overexpressing) or five exon 17b negative cells/field (siRNA knockdown) (10 fields for each sample; total 50 cells) were measured for both cell periphery length and E-cadherin–labeled length. The percentage of junction assembled was obtained by the ratio of the E-cadherin–labeled length over the length of the cell periphery.

To analyze the extent of actin and E-cadherin localization to cell–cell contact during calcium switch, the fluorescence intensity between cell–cell contacts and the cytoplasm for both proteins from the same frame was measured as described (78). In brief, the pixels from an area (6 × 1 μm) on cell–cell contacts and its adjacent area (6 × 1 μm) on the cytoplasm were obtained using ImageJ software. The ratio of fluorescence intensity (cell–cell contacts *versus* cytoplasm) for each time point for each protein during calcium switch was calculated from 50 cells.

Statistical analysis

Data were analyzed using GraphPad Prism 8 software (GraphPad Software, Inc., La Jolla, CA). All values were expressed as mean ± S.E. of the mean (S.E.). Statistical significance of quantitative data was determined by Student's *t* test. The level of significance difference was determined at $p < 0.001$.

Gel overlay assays

GST and ex17b/GST fusion proteins were affinity-purified via coupling to GSH-Sepharose beads, and ex17b was cleaved from ex17b/GST fusions using PreScission Protease (GE Healthcare). Gel overlay assays were performed as described previously (36). β-Actin and BSA were fractionated on a 12% SDS-polyacrylamide gel and either stained with Coomassie Blue dye or electrotransferred onto a PVDF membrane. The membrane was incubated in blocking buffer (50 mM Tris-HCl, pH 7.5, 140 mM NaCl, 0.1% Tween 20, 0.5% Nonidet P-40, 3% BSA, 0.5% gelatin, and 2 mM DTT) for 12 h at 4 °C and was overlaid with 3 μg/ml ex17b peptide in binding buffer (50 mM Tris-HCl, pH 7.5, 140 mM NaCl, 0.5% Nonidet P-40, 1% BSA, 0.25% gelatin, 2 mM ATP, and 2 mM DTT) for 3 h in 4 °C. The membrane was then washed with washing buffer (50 mM Tris-HCl, pH 7.5, 140 mM NaCl, 1.0% Nonidet P-40, and 2 mM DTT) and followed by Western blotting using an anti-ex17b antibody. For gel-overlay with actin, GST−17b and GST were fractionated on a 12% SDS-polyacrylamide gel, overlaid with biotinylated actin (Cytoskeleton, Inc.), incubated with streptavidin-horseradish peroxidase (Sigma), and developed using enhanced chemiluminescence.

Yeast two-hybrid assays

The Gal-4 based two-hybrid system encoding the Gal4-BD and Gal4-AD, respectively, was used to express hybrid proteins. To find proteins that interacted with the 4.1R exon 17b–encoded peptide, a human kidney cDNA library in Gal4-AD vector pACT2 (Clontech) was screened using either the full-length or the C-terminal region 100 amino acids of exon 17b cloned into Gal4-BD vector (pGBKT7) as the bait. They were co-transformed into yeast and assayed for β-gal activity on nitrocellulose filters as described in the Clontech manual. DNA from positive clones were amplified by standard PCR followed by DNA sequencing.

For mapping β-catenin armadillo domain repeats that interact with 4.1R–MBD, the MBD domain of 4.1R was inserted into pGBKT7 as the bait and the armadillo domain or its repeat-deletions were inserted into pGADT7 (1–12/pGADT7, 1–10/pGADT7, 1–8/pGADT7, 1–4/pGADT7, 1–2/pGADT7, 3–12/pGADT7, and 5–12/pGADT7) and analyzed. Co-transformation of p53/pGBKT7 and large T-antigen/pGADT7 served as a positive control. Negative controls were performed by transformation with pGBKT7-MBD or 1–12/pGADT7 alone.

Recombinant protein productions and GST-pulldown assays

4.1R/GST fusion and their deletion derivatives were affinity-purified via coupling to GSH-Sepharose beads (GE Healthcare) according to the manufacturer's protocol. Full-length β-catenin, its individual domains, and the armadillo repeat deletion derivatives cloned in pCl-neo or PCR-generated DNA fragments were used for *in vitro* transcription and translation using the TnT Quick Coupled Transcription/Translation System (Promega) in the presence of [^{35}S]methionine to radiolabel newly-synthesized proteins according to the manufacturer's protocol. GST-pulldown analyses were performed as reported previously (37) with modifications. TnT-produced proteins were incubated with 4.1R/GST fusion proteins coupled to Sepharose beads for 1 h at 4 °C in binding buffer (50 mM potassium phosphate, pH 7.3, 140 mM NaCl, 10 mM KCl). The mixture was washed five times with binding buffer in the presence of 1% Triton X-100, and the bound proteins were analyzed on a gel, treated with Enlightening (PerkinElmer Life Sciences), and visualized by fluorography.

For actin pulldown, 5 μM GST or 17b/GST fusion proteins were incubated with 5 μM actin in 60 μl of binding buffer (20 mM Tris-HCl, 200 mM NaCl, 1 mM EDTA, 0.5% Nonidet P-40, pH 8.0) at 4 °C for 2 h. The protein mix was incubated with 60 μl of GSH-agarose beads for an additional 1 h. The beads were then washed four times with a washing buffer (20 mM Tris-HCl, 20 mM KCl, 0.1% Triton X-100, 1 mM DTT, pH 8.0). The presence of actin bound to 17b/GST was detected by Western blotting using an anti-β-actin Ab.

Co-sedimentation assays

Commercially obtained F-actin was polymerized at a concentration of 1 mg/ml, according to the manufacturer's instructions (Cytoskeleton, Denver, CO). Fodrin purification from rat brain was carried out as described (36). Purified brain fodrin, recombinant GST fusion polypeptides, and F-actin were subsequently dialyzed against several changes of binding buffer (130 mM KCl, 25 mM NaCl, 2 mM $MgCl_2$, 0.4 mM DTT, 0.2 mM $CaCl_2$, 20 mM Hepes, pH 7.2) (79) at 4 °C. Co-sedimentation assays were performed in 50 μl of binding buffer in the presence of 0.2 μM fodrin, 5.7 μM F-actin, and 1.4 μM GST–Ex16/17, GST–Ex17, GST–Ex17/17b, GST–Ex17b, or GST-alone polypeptides. The reaction mixtures were incubated at room temperature for 45 min and then centrifuged at 4 °C for 1 h at 100,000 × *g* in a Beckman 42.2Ti rotor. Equivalent portions of supernatants and pellets were subsequently fractionated by 10% SDS-PAGE.

Author contributions—S.-C. H. and E. J. B. conceptualization; S.-C. H. and E. J. B. supervision; S.-C. H. and E. J. B. funding acquisition; S.-C. H., J. Y. L., L. V. V., F. H. Y., A. C. O., J. P. O., and H. S. Z. validation; S.-C. H., J. Y. L., L. V. V., F. H. Y., A. C. O., J. P. O., and H. S. Z. investigation; S.-C. H. writing-original draft; S.-C. H. and E. J. B. project administration; J. Y. L., L. V. V., F. H. Y., A. C. O., J. P. O., H. S. Z., and K. M. B. data curation; J. Y. L., L. V. V., F. H. Y., A. C. O., J. P. O., and H. S. Z. formal analysis; J. Y. L., L. V. V., F. H. Y., A. C. O., J. P. O., and H. S. Z. visualization; J. Y. L., L. V. V., F. H. Y., A. C. O., J. P. O., and H. S. Z. methodology; E. J. B. writing-review and editing.

Acknowledgments—We thank Drs. Alan Fanning and James Anderson (University of North Carolina, Chapel Hill) for the MDCK II cells. We also thank Rodrigo Bustos and Lin Chen for initial studies and Indira Munagala and Anyu Zhou for technical assistance.

References

1. Bryant, D. M., and Mostov, K. E. (2008) From cells to organs: building polarized tissue. *Nat. Rev. Mol. Cell Biol.* **9,** 887–901 CrossRef Medline
2. Farquhar, M. G., and Palade, G. E. (1963) Junctional complexes in various epithelia. *J. Cell Biol.* **17,** 375–412 CrossRef Medline
3. Yap, A. S., Brieher, W. M., Pruschy, M., and Gumbiner, B. M. (1997) Lateral clustering of the adhesive ectodomain: a fundamental determinant of cadherin function. *Curr. Biol.* **7,** 308–315 CrossRef Medline
4. Garcia, M. A., Nelson, W. J., and Chavez, N. (2018) Cell–cell junctions organize structural and signaling networks. *Cold Spring Harb. Perspect. Biol.* **10,** a029181 CrossRef Medline
5. Hartsock, A., and Nelson, W. J. (2008) Adherens and tight junctions: structure, function and connections to the actin cytoskeleton. *Biochim. Biophys. Acta* **1778,** 660–669 CrossRef Medline
6. Pokutta, S., and Weis, W. I. (2007) Structure and mechanism of cadherins and catenins in cell–cell contacts. *Annu. Rev. Cell Dev. Biol.* **23,** 237–261 CrossRef Medline
7. Adams, C. L., and Nelson, W. J. (1998) Cytomechanics of cadherin-mediated cell–cell adhesion. *Curr. Opin. Cell Biol.* **10,** 572–577 CrossRef Medline
8. D'Souza-Schorey, C. (2005) Disassembling adherens junctions: breaking up is hard to do. *Trends Cell Biol.* **15,** 19–26 CrossRef Medline
9. Cavey, M., and Lecuit, T. (2009) Molecular bases of cell–cell junctions stability and dynamics. *Cold Spring Harb. Perspect. Biol.* **1, a002998** CrossRef Medline
10. Ivanov, A. I. (2008) Actin motors that drive formation and disassembly of epithelial apical junctions. *Front. Biosci.* **13,** 6662–6681 CrossRef Medline
11. Ivanov, A. I., Nusrat, A., and Parkos, C. A. (2005) Endocytosis of the apical junctional complex: mechanisms and possible roles in regulation of epithelial barriers. *Bioessays* **27,** 356–365 CrossRef Medline
12. Turner, J. R. (2009) Intestinal mucosal barrier function in health and disease. *Nat. Rev. Immunol.* **9,** 799–809 CrossRef Medline
13. Mège, R. M., Gavard, J., and Lambert, M. (2006) Regulation of cell–cell junctions by the cytoskeleton. *Curr. Opin. Cell Biol.* **18,** 541–548 CrossRef Medline

14. Perez-Moreno, M., Jamora, C., and Fuchs, E. (2003) Sticky business: orchestrating cellular signals at adherens junctions. *Cell* **112,** 535–548 CrossRef Medline
15. Ma, T. Y., Hollander, D., Tran, L. T., Nguyen, D., Hoa, N., and Bhalla, D. (1995) Cytoskeletal regulation of Caco-2 intestinal monolayer paracellular permeability. *J. Cell. Physiol.* **164,** 533–545 CrossRef Medline
16. Ivanov, A. I., McCall, I. C., Parkos, C. A., and Nusrat, A. (2004) Role for actin filament turnover and a myosin II motor in cytoskeleton-driven disassembly of the epithelial apical junctional complex. *Mol. Biol. Cell* **15,** 2639–2651 CrossRef Medline
17. Vasioukhin, V., Bauer, C., Yin, M., and Fuchs, E. (2000) Directed actin polymerization is the driving force for epithelial cell–cell adhesion. *Cell* **100,** 209–219 CrossRef Medline
18. Zhang, J., Betson, M., Erasmus, J., Zeikos, K., Bailly, M., Cramer, L. P., and Braga, V. M. (2005) Actin at cell–cell junctions is composed of two dynamic and functional populations. *J. Cell Sci.* **118,** 5549–5562 CrossRef Medline
19. Kobielak, A., Pasolli, H. A., and Fuchs, E. (2004) Mammalian formin-1 participates in adherens junctions and polymerization of linear actin cables. *Nat. Cell Biol.* **6,** 21–30 CrossRef Medline
20. Boguslavsky, S., Grosheva, I., Landau, E., Shtutman, M., Cohen, M., Arnold, K., Feinstein, E., Geiger, B., and Bershadsky, A. (2007) p120 catenin regulates lamellipodial dynamics and cell adhesion in cooperation with cortactin. *Proc. Natl. Acad. Sci. U.S.A.* **104,** 10882–10887 CrossRef Medline
21. Helwani, F. M., Kovacs, E. M., Paterson, A. D., Verma, S., Ali, R. G., Fanning, A. S., Weed, S. A., and Yap, A. S. (2004) Cortactin is necessary for E-cadherin-mediated contact formation and actin reorganization. *J. Cell Biol.* **164,** 899–910 CrossRef Medline
22. Bennett, V., and Baines, A. J. (2001) Spectrin and ankyrin-based pathways: metazoan inventions for integrating cells into tissues. *Physiol. Rev.* **81,** 1353–1392 CrossRef Medline
23. Baines, A. J. (2009) Evolution of spectrin function in cytoskeletal and membrane networks. *Biochem. Soc. Trans.* **37,** 796–803 CrossRef Medline
24. Pradhan, D., Lombardo, C. R., Roe, S., Rimm, D. L., and Morrow, J. S. (2001) α-Catenin binds directly to spectrin and facilitates spectrin–membrane assembly *in vivo*. *J. Biol. Chem.* **276,** 4175–4181 CrossRef Medline
25. Zarnescu, D. C., and Thomas, G. H. (1999) Apical spectrin is essential for epithelial morphogenesis but not apicobasal polarity in *Drosophila*. *J. Cell Biol.* **146,** 1075–1086 CrossRef Medline
26. Naydenov, N. G., and Ivanov, A. I. (2010) Adducins regulate remodeling of apical junctions in human epithelial cells. *Mol. Biol. Cell* **21,** 3506–3517 CrossRef Medline
27. Kizhatil, K., Davis, J. Q., Davis, L., Hoffman, J., Hogan, B. L., and Bennett, V. (2007) Ankyrin-G is a molecular partner of E-cadherin in epithelial cells and early embryos. *J. Biol. Chem.* **282,** 26552–26561 CrossRef Medline
28. Naydenov, N. G., and Ivanov, A. I. (2011) Spectrin–adducin membrane skeleton: a missing link between epithelial junctions and the actin cytoskeleton? *Bioarchitecture* **1,** 186–191 CrossRef Medline
29. Baines, A. J., Lu, H. C., and Bennett, P. M. (2014) The protein 4.1 family: hub proteins in animals for organizing membrane proteins. *Biochim. Biophys. Acta* **1838,** 605–619 CrossRef Medline
30. Lallemand, D., Curto, M., Saotome, I., Giovannini, M., and McClatchey, A. I. (2003) NF2 deficiency promotes tumorigenesis and metastasis by destabilizing adherens junctions. *Genes Dev.* **17,** 1090–1100 CrossRef Medline
31. Scoles, D. R., Huynh, D. P., Morcos, P. A., Coulsell, E. R., Robinson, N. G., Tamanoi, F., and Pulst, S. M. (1998) Neurofibromatosis 2 tumour suppressor schwannomin interacts with βII-spectrin. *Nat. Genet.* **18,** 354–359 CrossRef Medline
32. Kuhlman, P. A., Hughes, C. A., Bennett, V., and Fowler, V. M. (1996) A new function for adducin. Calcium/calmodulin-regulated capping of the barbed ends of actin filaments. *J. Biol. Chem.* **271,** 7986–7991 CrossRef Medline
33. Mische, S. M., Mooseker, M. S., and Morrow, J. S. (1987) Erythrocyte adducin: a calmodulin-regulated actin-bundling protein that stimulates spectrin–actin binding. *J. Cell Biol.* **105,** 2837–2845 CrossRef Medline
34. Correas, I., Leto, T. L., Speicher, D. W., and Marchesi, V. T. (1986) Identification of the functional site of erythrocyte protein 4.1 involved in spectrin–actin associations. *J. Biol. Chem.* **261,** 3310–3315 Medline
35. Schischmanoff, P. O., Winardi, R., Discher, D. E., Parra, M. K., Bicknese, S. E., Witkowska, H. E., Conboy, J. G., and Mohandas, N. (1995) Defining of the minimal domain of protein 4.1 involved in spectrin–actin binding. *J. Biol. Chem.* **270,** 21243–21250 CrossRef Medline
36. Kontrogianni-Konstantopoulos, A., Frye, C. S., Benz, E. J., Jr., and Huang, S. C. (2001) The prototypical 4.1R–10-kDa domain and the 4.1g–10-kDa paralog mediate fodrin–actin complex formation. *J. Biol. Chem.* **276,** 20679–20687 CrossRef Medline
37. Mattagajasingh, S. N., Huang, S. C., Hartenstein, J. S., and Benz, E. J., Jr. (2000) Characterization of the interaction between protein 4.1R and ZO-2. A possible link between the tight junction and the actin cytoskeleton. *J. Biol. Chem.* **275,** 30573–30585 CrossRef Medline
38. Yang, S., Guo, X., Debnath, G., Mohandas, N., and An, X. (2009) Protein 4.1R links E-cadherin/β-catenin complex to the cytoskeleton through its direct interaction with β-catenin and modulates adherens junction integrity. *Biochim. Biophys. Acta* **1788,** 1458–1465 CrossRef Medline
39. Schischmanoff, P. O., Yaswen, P., Parra, M. K., Lee, G., Chasis, J. A., Mohandas, N., and Conboy, J. G. (1997) Cell shape-dependent regulation of protein 4.1 alternative pre-mRNA splicing in mammary epithelial cells. *J. Biol. Chem.* **272,** 10254–10259 CrossRef Medline
40. Lallena, M. J., Martínez, C., Valcárcel, J., and Correas, I. (1998) Functional association of nuclear protein 4.1 with pre-mRNA splicing factors. *J. Cell Sci.* **111,** 1963–1971 Medline
41. Krauss, S. W., Heald, R., Lee, G., Nunomura, W., Gimm, J. A., Mohandas, N., and Chasis, J. A. (2002) Two distinct domains of protein 4.1 critical for assembly of functional nuclei *in vitro*. *J. Biol. Chem.* **277,** 44339–44346 CrossRef Medline
42. Mattagajasingh, S. N., Huang, S. C., Hartenstein, J. S., Snyder, M., Marchesi, V. T., and Benz, E. J. (1999) A nonerythroid isoform of protein 4.1R interacts with the nuclear mitotic apparatus (NuMA) protein. *J. Cell Biol.* **145,** 29–43 CrossRef Medline
43. Huang, S. C., Liu, E. S., Chan, S. H., Munagala, I. D., Cho, H. T., Jagadeeswaran, R., and Benz, E. J., Jr. (2005) Mitotic regulation of protein 4.1R involves phosphorylation by cdc2 kinase. *Mol. Biol. Cell* **16,** 117–127 CrossRef Medline
44. Kontrogianni-Konstantopoulos, A., Huang, S. C., and Benz, E J., Jr. (2000) A nonerythroid isoform of protein 4.1R interacts with components of the contractile apparatus in skeletal myofibers. *Mol. Biol. Cell* **11,** 3805–3817 CrossRef Medline
45. Wheelock, M. J., Shintani, Y., Maeda, M., Fukumoto, Y., and Johnson, K. R. (2008) Cadherin switching. *J. Cell Sci.* **121,** 727–735 CrossRef Medline
46. Wang, R., Chen, Y. S., Dashwood, W. M., Li, Q., Löhr, C. V., Fischer, K., Ho, E., Williams, D. E., and Dashwood, R. H. (2017) Divergent roles of p120-catenin isoforms linked to altered cell viability, proliferation, and invasiveness in carcinogen-induced rat skin tumors. *Mol. Carcinog.* **56,** 1733–1742 CrossRef Medline
47. Maruo, T., Sakakibara, S., Miyata, M., Itoh, Y., Kurita, S., Mandai, K., Sasaki, T., and Takai, Y. (2018) Involvement of l-afadin, but not s-afadin, in the formation of puncta adherentia junctions of hippocampal synapses. *Mol. Cell. Neurosci.* **92,** 40–49 CrossRef Medline
48. Parra, M. K., Gee, S. L., Koury, M. J., Mohandas, N., and Conboy, J. G. (2003) Alternative 5′ exons and differential splicing regulate expression of protein 4.1R isoforms with distinct N termini. *Blood* **101,** 4164–4171 CrossRef Medline
49. Huang, S. C., Cho, A., Norton, S., Liu, E. S., Park, J., Zhou, A., Munagala, I. D., Ou, A. C., Yang, G., Wickrema, A., Tang, T. K., and Benz, E. J., Jr. (2009) Coupled transcription-splicing regulation of mutually exclusive splicing events at the 5′ exons of protein 4.1R gene. *Blood* **114,** 4233–4242 CrossRef Medline
50. Deguillien, M., Huang, S. C., Morinière, M., Dreumont, N., Benz, E. J., Jr., and Baklouti, F. (2001) Multiple cis elements regulate an alternative splic-

ing event at 4.1R pre-mRNA during erythroid differentiation. *Blood* **98,** 3809–3816 CrossRef Medline

51. Seo, P. S., Jeong, J. J., Zeng, L., Takoudis, C. G., Quinn, B. J., Khan, A. A., Hanada, T., and Chishti, A. H. (2009) Alternatively spliced exon 5 of the FERM domain of protein 4.1R encodes a novel binding site for erythrocyte p55 and is critical for membrane targeting in epithelial cells. *Biochim. Biophys. Acta* **1793,** 281–289 CrossRef Medline
52. Megy, S., Bertho, G., Gharbi-Benarous, J., Evrard-Todeschi, N., Coadou, G., Ségéral, E., Iehle, C., Quéméneur, E., Benarous, R., and Girault, J. P. (2005) STD and TRNOESY NMR studies on the conformation of the oncogenic protein β-catenin containing the phosphorylated motif DpS-G*XX*pS bound to the β-TrCP protein. *J. Biol. Chem.* **280,** 29107–29116 CrossRef Medline
53. Xu, W., and Kimelman, D. (2007) Mechanistic insights from structural studies of β-catenin and its binding partners. *J. Cell Sci.* **120,** 3337–3344 CrossRef Medline
54. Capaldo, C. T., and Macara, I. G. (2007) Depletion of E-cadherin disrupts establishment but not maintenance of cell junctions in Madin-Darby canine kidney epithelial cells. *Mol. Biol. Cell* **18,** 189–200 CrossRef Medline
55. Baranwal, S., Naydenov, N. G., Harris, G., Dugina, V., Morgan, K. G., Chaponnier, C., and Ivanov, A. I. (2012) Nonredundant roles of cytoplasmic β- and γ-actin isoforms in regulation of epithelial apical junctions. *Mol. Biol. Cell* **23,** 3542–3553 CrossRef Medline
56. Schumann, D., Chen, C. J., Kaplan, B., and Shively, J. E. (2001) Carcinoembryonic antigen cell adhesion molecule 1 directly associates with cytoskeleton proteins actin and tropomyosin. *J. Biol. Chem.* **276,** 47421–47433 CrossRef Medline
57. Wang, C. L., Wang, L. W., Xu, S. A., Lu, R. C., Saavedra-Alanis, V., and Bryan, J. (1991) Localization of the calmodulin- and the actin-binding sites of caldesmon. *J. Biol. Chem.* **266,** 9166–9172 Medline
58. Vandekerckhove, J., and Vancompernolle, K. (1992) Structural relationships of actin-binding proteins. *Curr. Opin. Cell Biol.* **4,** 36–42 CrossRef Medline
59. Friederich, E., Vancompernolle, K., Huet, C., Goethals, M., Finidori, J., Vandekerckhove, J., and Louvard, D. (1992) An actin-binding site containing a conserved motif of charged amino acid residues is essential for the morphogenic effect of villin. *Cell* **70,** 81–92 CrossRef Medline
60. Zhang, J., Yang, S., An, C., Wang, J., Yan, H., Huang, Y., Song, J., Yin, C., Baines, A. J., Mohandas, N., and An, X. (2014) Comprehensive characterization of protein 4.1 expression in epithelium of large intestine. *Histochem. Cell Biol.* **142,** 529–539 CrossRef Medline
61. Shi, Z. T., Afzal, V., Coller, B., Patel, D., Chasis, J. A., Parra, M., Lee, G., Paszty, C., Stevens, M., Walensky, L., Peters, L. L., Mohandas, N., Rubin, E., and Conboy, J. G. (1999) Protein 4.1R-deficient mice are viable but have erythroid membrane skeleton abnormalities. *J. Clin. Invest.* **103,** 331–340 CrossRef Medline
62. Tyler, J. M., Reinhardt, B. N., and Branton, D. (1980) Associations of erythrocyte membrane proteins: binding of purified bands 2.1 and 4.1 to spectrin. *J. Biol. Chem.* **255,** 7034–7039 Medline
63. Fowler, V., and Taylor, D. L. (1980) Spectrin plus band 4.1 crosslink actin: regulation by micromolar calcium. *J. Cell Biol.* **85,** 361–376 CrossRef Medline
64. Gascard, P., Nunomura, W., Lee, G., Walensky, L. D., Krauss, S. W., Takakuwa, Y., Chasis, J. A., Mohandas, N., and Conboy, J. G. (1999) Deciphering the nuclear import pathway for the cytoskeletal red cell protein 4.1R. *Mol. Biol. Cell* **10,** 1783–1798 CrossRef Medline
65. Ponthier, J. L., Schluepen, C., Chen, W., Lersch, R. A., Gee, S. L., Hou, V. C., Lo, A. J., Short, S. A., Chasis, J. A., Winkelmann, J. C., and Conboy, J. G. (2006) Fox-2 splicing factor binds to a conserved intron motif to promote inclusion of protein 4.1R alternative exon 16. *J. Biol. Chem.* **281,** 12468–12474 CrossRef Medline
66. Shaw, R. J., Paez, J. G., Curto, M., Yaktine, A., Pruitt, W. M., Saotome, I., O'Bryan, J. P., Gupta, V., Ratner, N., Der, C. J., Jacks, T., and McClatchey, A. I. (2001) The Nf2 tumor suppressor, merlin, functions in Rac-dependent signaling. *Dev. Cell* **1,** 63–72 CrossRef Medline
67. Bretscher, A., Edwards, K., and Fehon, R. G. (2002) ERM proteins and merlin: integrators at the cell cortex. *Nat. Rev. Mol. Cell Biol.* **3,** 586–599 CrossRef Medline
68. Perry, A., Gutmann, D. H., and Reifenberger, G. (2004) Molecular pathogenesis of meningiomas. *J. Neurooncol.* **70,** 183–202 CrossRef Medline
69. Robb, V. A., Li, W., Gascard, P., Perry, A., Mohandas, N., and Gutmann, D. H. (2003) Identification of a third protein 4.1 tumor suppressor, protein 4.1R, in meningioma pathogenesis. *Neurobiol. Dis.* **13,** 191–202 CrossRef Medline
70. Rajaram, V., Gutmann, D. H., Prasad, S. K., Mansur, D. B., and Perry, A. (2005) Alterations of protein 4.1 family members in ependymomas: a study of 84 cases. *Mod. Pathol.* **18,** 991–997 CrossRef Medline
71. Pećina-Šlaus, N. (2013) Merlin, the NF2 gene product. *Pathol. Oncol. Res.* **19,** 365–373 CrossRef Medline
72. Lekanne Deprez, R. H., Bianchi, A. B., Groen, N. A., Seizinger, B. R., Hagemeijer, A., van Drunen, E., Bootsma, D., Koper, J. W., Avezaat, C. J., and Kley, N. (1994) Frequent NF2 gene transcript mutations in sporadic meningiomas and vestibular schwannomas. *Am. J. Hum. Genet.* **54,** 1022–1029 Medline
73. Huynh, D. P., Mautner, V., Baser, M. E., Stavrou, D., and Pulst, S. M. (1997) Immunohistochemical detection of schwannomin and neurofibromin in vestibular schwannomas, ependymomas, and meningiomas. *J. Neuropathol. Exp. Neurol.* **56,** 382–390 CrossRef Medline
74. James, M. F., Manchanda, N., Gonzalez-Agosti, C., Hartwig, J. H., and Ramesh, V. (2001) The neurofibromatosis 2 protein product merlin selectively binds F-actin but not G-actin, and stabilizes the filaments through a lateral association. *Biochem. J.* **356,** 377–386 CrossRef Medline
75. Gladden, A. B., Hebert, A. M., Schneeberger, E. E., and McClatchey, A. I. (2010) The NF2 tumor suppressor, Merlin, regulates epidermal development through the establishment of a junctional polarity complex. *Dev. Cell* **19,** 727–739 CrossRef Medline
76. Huang, S. C., Zhou, A., Nguyen, D. T., Zhang, H. S., and Benz, E. J., Jr. (2016) Protein 4.1R influences myogenin protein stability and skeletal muscle differentiation. *J. Biol. Chem.* **291,** 25591–25607 CrossRef Medline
77. Guerrera, D., Shah, J., Vasileva, E., Sluysmans, S., Méan, I., Jond, L., Poser, I., Mann, M., Hyman, A. A., and Citi, S. (2016) PLEKHA7 recruits PDZD11 to adherens junctions to stabilize nectins. *J. Biol. Chem.* **291,** 11016–11029 CrossRef Medline
78. Chen, C. L., and Chen, H. C. (2009) Functional suppression of E-cadherin by protein kinase Cδ. *J. Cell Sci.* **122,** 513–523 CrossRef Medline
79. Harris, A. S., and Morrow, J. S. (1990) Calmodulin and calcium-dependent protease I coordinately regulate the interaction of fodrin with actin. *Proc. Natl. Acad. Sci. U.S.A.* **87,** 3009–3013 CrossRef Medline